cmgh
CELLULAR AND MOLECULAR GASTROENTEROLOGY AND HEPATOLOGY

ORIGINAL RESEARCH

Acetyl-CoA Carboxylase Inhibition Improves Multiple Dimensions of NASH Pathogenesis in Model Systems

Trenton T. Ross,[1] Collin Crowley,[1] Kenneth L. Kelly,[1] Anthony Rinaldi,[1] David A. Beebe,[1] Matthew P. Lech,[2] Robert V. Martinez,[2] Santos Carvajal-Gonzalez,[3] Magalie Boucher,[4] Dinesh Hirenallur-Shanthappa,[5] Jeffrey Morin,[5] Alan C. Opsahl,[4] Sarah R. Vargas,[4] Kendra K. Bence,[1] Jeffrey A. Pfefferkorn,[1] and William P. Esler[1]

[1]Internal Medicine Research Unit, [2]Inflammation and Immunology Research Unit, [3]Early Clinical Development, [4]Drug Safety Research and Development, [5]Comparative Medicine, Pfizer Worldwide Research and Development, Cambridge Massachusetts

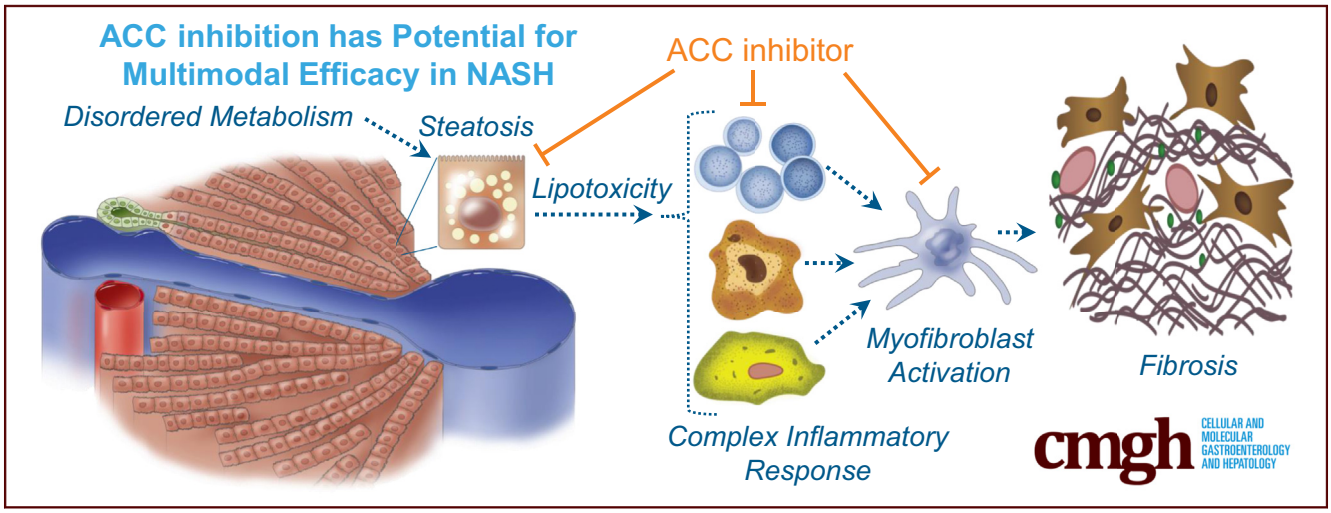

SUMMARY

The pathogenesis of nonalcoholic steatohepatitis is multifactorial, involving steatosis, lipotoxicity, hepatic inflammation, and fibrosis. The present studies show that acetyl-CoA carboxylase inhibition produces direct improvements in hepatic steatosis, inflammation, and fibrosis in both primary human cell systems and rodent nonalcoholic fatty liver disease/nonalcoholic steatohepatitis models.

BACKGROUND & AIMS: Disordered metabolism, steatosis, hepatic inflammation, and fibrosis contribute to the pathogenesis of nonalcoholic steatohepatitis (NASH). Acetyl-CoA carboxylase (ACC) catalyzes the first committed step in de novo lipogenesis (DNL) and modulates mitochondrial fatty acid oxidation. Increased hepatic DNL flux and reduced fatty acid oxidation are hypothesized to contribute to steatosis. Some proinflammatory cells also show increased dependency on DNL, suggesting that ACC may regulate aspects of the inflammatory response in NASH. PF-05221304 is an orally bioavailable, liver-directed ACC1/2 inhibitor. The present studies sought to evaluate the effects of PF-05221304 on NASH pathogenic factors in experimental model systems.

METHODS: The effects of PF-05221304 on lipid metabolism, steatosis, inflammation, and fibrogenesis were investigated in both primary human-derived in vitro systems and in vivo rodent models.

RESULTS: PF-05221304 inhibited DNL, stimulated fatty acid oxidation, and reduced triglyceride accumulation in primary human hepatocytes, and reduced DNL and steatosis in Western diet–fed rats in vivo, showing the potential to reduce hepatic lipid accumulation and potentially lipotoxicity. PF-05221304 blocked polarization of human T cells to proinflammatory but not anti-inflammatory T cells, and suppressed activation of primary human stellate cells to myofibroblasts in vitro, showing direct effects on inflammation and fibrogenesis. Consistent with these observations, PF-05221304 also reduced markers of inflammation and fibrosis in the diethylnitrosamine chemical–induced liver injury model and the choline-deficient, high-fat–fed rat model.

CONCLUSIONS: The liver-directed dual ACC1/ACC2 inhibitor directly improved multiple nonalcoholic fatty liver disease/NASH pathogenic factors including steatosis, inflammation, and fibrosis in both human-derived in vitro systems and rat models. *(Cell Mol Gastroenterol Hepatol 2020;10:829–851; https://doi.org/10.1016/j.jcmgh.2020.06.001)*

Keywords: Fatty Liver Disease; NASH; Lipogenesis; Fibrosis; Acetyl-CoA Carboxylase.

Nonalcoholic fatty liver disease (NAFLD) is a continuum of liver disorders characterized by excessive accumulation of fat (in excess of 5%) within the hepatocytes.[1] Nonalcoholic steatohepatitis (NASH) is a clinical and histologic subset of NAFLD that is characterized histologically by the presence of liver injury and inflammation with or without varying degrees of fibrosis.[1] NASH is associated with increased all-cause mortality, cirrhosis and end-stage liver disease, increased cardiovascular mortality, and increased incidence of both liver and non–liver-related cancers.[1] The molecular etiology of NASH is complex, involving multiple contributing pathogenic factors including disordered metabolism leading to development of steatosis and lipotoxicity, a complex immune response, hepatocyte injury, and activation of hepatic stellate cells leading to the development of progressive fibrosis. Pharmacologic agents, or combinations of pharmacologic agents, that address multiple aspects of this pathogenic cascade may be particularly valuable for therapeutic intervention in NASH given this complex and multifactorial disease pathogenesis.[2]

Hepatic steatosis is a consequence of an imbalance in triglyceride (TG) production/uptake into the liver and clearance/removal.[3] Increased rates of hepatic de novo lipogenesis (DNL) have been reported to be a distinctive characteristic of NAFLD.[4] Human subjects with increased liver fat showed an approximately 3-fold increase in the rate of hepatic DNL relative to subjects with normal liver fat. Altering the balance of hepatic TG accumulation and removal by either (or both) reducing fat production or promoting fat clearance is expected to reduce steatosis. Acetyl-CoA carboxylase (ACC) is a key enzyme regulating lipid metabolism,[5] catalyzing the adenosine triphosphate (ATP)-dependent condensation of acetyl-CoA with carbonate to produce malonyl-CoA.[6] The malonyl-CoA is an essential substrate for DNL and regulates β oxidation through allosteric inhibition of carnitine palmitoyltransferase 1.[5,7] There are 2 isoforms of ACC: ACC1 and ACC2. ACC inhibition stimulates fatty acid oxidation, suppresses hepatic DNL, and consequently reduces steatosis.[8,9] Amelioration of steatosis in turn is hypothesized to suppress hepatic inflammation and subsequently reduce fibrogenesis. In addition, emerging data also suggest that suppression of DNL through ACC inhibition may directly reduce inflammation by restraining the formation of the inflammatory interleukin 17–secreting T cells of the T helper 17 lineage (TH17 cells) and promoting the development of anti-inflammatory Foxp3(+) regulatory T (Treg) cells.[10] Studies comparing human subjects with NASH vs those with simple steatosis or healthy liver have shown that progression from NAFLD to NASH is marked by a higher frequency of Th17 cells in the liver and an increase in the ratio of Th17 cells to Treg cells in peripheral blood and in the liver.[11]

PF-05221304 is a potent, orally bioavailable, dual acetyl-CoA carboxylase (ACC1/ACC2) inhibitor and is also a substrate of the organic anion transporting polypeptides, leading to asymmetrical tissue distribution and increased concentrations in the liver relative to plasma and other tissues.[12] In the present studies, we sought to probe the effects of PF-05221304 on steatosis, hepatic inflammation, and fibrosis in both primary human-derived in vitro systems and rodent in vivo models.

Results

PF-05221304 Is a Potent, Reversible ACC1/2 Inhibitor

The structure of PF-05221304 is shown in Figure 1*A*. The reversibility of PF-05221304 inhibition of human ACC1 was shown by a change in reaction velocity after dilution under conditions that maintained constant substrate concentrations (Figure 1*B*). Lineweaver–Burk analyses (Figure 1*C*–*E*) show that inhibition of human ACC (hACC)1 by PF-05221304 is noncompetitive with respect to ATP and noncompetitive with respect to acetyl-CoA and bicarbonate. PF-05221304 inhibited rat (Figure 1*F*) and human (Figure 1*G*) ACC1 and ACC2 with median inhibitory concentration (IC_{50}) values of 7.5 ± 0.7 nmol/L for rat ACC1, 8.2 ± 4.1 nmol/L for rat ACC2, 12.4 ± 1.4 nmol/L for human ACC1, and 8.7 ± 2.5 nmol/L for human ACC2.

PF-05221304 Inhibits DNL, Increases β-Oxidation, and Reduces Triglyceride Accumulation in Primary Human Hepatocytes

PF-05221304 produced concentration-dependent inhibition of DNL in primary human hepatocytes with an IC_{50} of 61 nmol/L (Figure 2*A*). At the nadir, PF-05221304 inhibited DNL by 77%. Administration of PF-05221304 to primary human hepatocytes resulted in increased fatty acid oxidation by 127% ($P < .05$) relative to cells administered vehicle, which was defined as 100% (Figure 2*B*).

Administration of PF-05221304 to hepatocytes cultured in the presence of high insulin and glucose significantly reduced total hepatic TG levels at 24 and 48 hours after administration by 47% ($P < .05$) relative to vehicle-treated hepatocytes (Figure 2*C*). Specifically, PF-05221304 significantly reduced TG species typically composed of de novo–derived fatty acids, including tripalmitin ($P < .05$) and tristearin ($P < .05$) (Figure 2*D*). In contrast, PF-05221304

Abbreviations used in this paper: **ACC, acetyl-CoA carboxylase; ALT, alanine aminotransferase; αSMA, α-smooth muscle actin; AST, aspartate aminotransferase; ATP, adenosine triphosphate; CD3, cluster of differentiation 3; CDAHFD, choline-deficient and high-fat diet; DAB, 3,3′-diaminobenzidine; DEN, diethylnitrosamine; DMSO, dimethyl sulfoxide; DNL, de novo lipogenesis; EC_{50}, median effective concentration; hACC, human ACC; HSC, primary hepatic stellate cell; IC_{50}, median inhibitory concentration; IHC, immunohistochemistry; IL, interleukin; NAFLD, nonalcoholic fatty liver disease; NASH, nonalcoholic steatohepatitis; PSR, Picro Sirius red; SWE, shear wave elastography; TG, triglyceride; TGFβ1, transforming growth factor β1; TH17 cells, inflammatory interleukin 17 secreting T cells of the T helper 17 lineage; Treg cells, anti-inflammatory Foxp3(+) regulatory T cells; VLDL, very-low-density lipoprotein.**

Most current article

2352-345X
https://doi.org/10.1016/j.jcmgh.2020.06.001

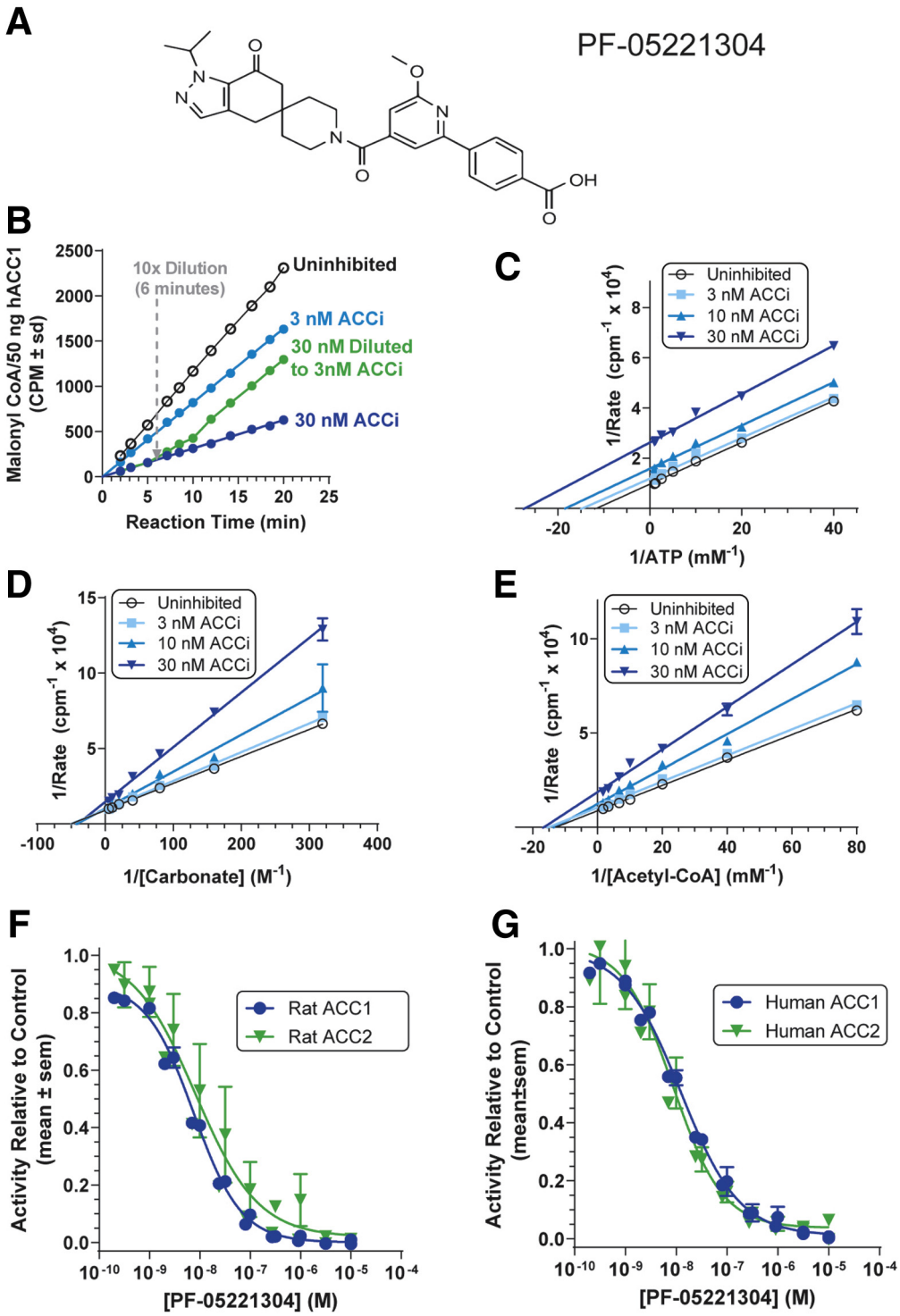

Figure 1. Characterization of ACC inhibition by PF-05221304. (*A*) Chemical structure of PF-05221304. (*B*) Reversibility of PF-05221304 binding by dilution. (*C*) Lineweaver–Burk analysis of PF-05221304 with ATP as the varied substrate. (*D*) Lineweaver–Burk analysis of PF-05221304 with carbonate as the varied substrate. (*E*) Lineweaver–Burk analysis of PF-05221304 with acetyl-CoA as the varied substrate. (*C–D*) *Open circles*, uninhibited; *squares*, 3 nmol/L PF-05221304; *triangles*, 10 nmol/L PF-05221304; *reverse triangles*, 30 nmol/L PF-05221304. (*F* and *G*) Inhibition dose curves for (*F*) rat and (*G*) human ACC isoforms. ACCi, PF-05221304.

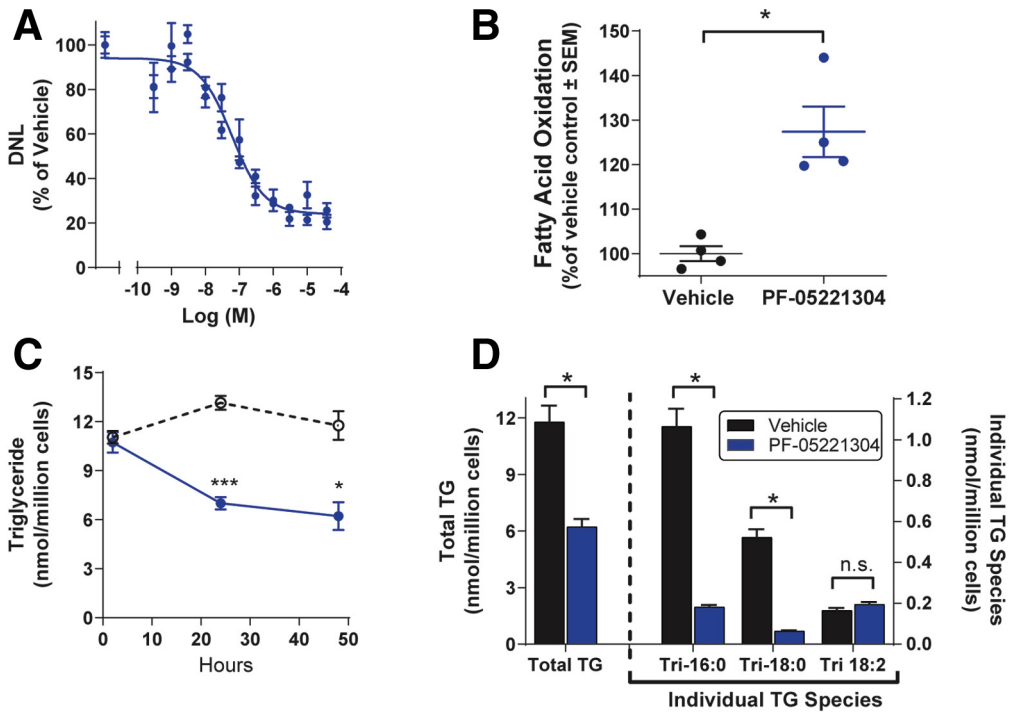

Figure 2. Effects of PF-05221304 on de novo lipogenesis, fatty acid oxidation, and triglyceride accumulation in primary human hepatocytes. (*A*) PF-05221304 suppressed DNL, as assessed by incorporation of ^{14}C acetate into lipids in a concentration-dependent manner. (*B*) PF-05221304 (*closed circles*) stimulated hepatocyte fatty acid oxidation relative to vehicle (*open circles*) as measured by production of $^{3}H_2O$ from ^{3}H-palmitate. (*C*) Accumulation of total hepatocyte triglyceride levels were suppressed by PF-05221304 (*closed circles*) relative to vehicle (*open circles*). (*D*) Relative to vehicle, PF-05221304 suppressed levels of total triglycerides, tripalmitin (Tri-16:0), and tristate (Tri-18:0), but not trilinolein (Tri-18:2). *$P < .05$ relative to vehicle. ***$P < .001$ relative to vehicle.

did not alter levels of trilinolein, a TG species composed of a dietary essential fatty acid that cannot be synthesized de novo (Figure 2*D*), suggesting that PF-05221304 suppressed hepatocyte TG accumulation largely by inhibiting DNL.

PF-05221304 Inhibits Malonyl-CoA Production, Suppresses Hepatic DNL, and Reduces Steatosis in Rats

Acute oral administration of PF-05221304 to chow-fed rats produced dose-dependent reductions in hepatic malonyl-CoA and hepatic DNL (Figure 3*A* and *B*). The median effective dose for the inhibition of hepatic malonyl-CoA was 5 mg/kg (Figure 3*A*). At the nadir, malonyl-CoA was inhibited by 85%. The median effective dose for the inhibition of hepatic DNL was 7 mg/kg (Figure 3*B*). At the nadir, hepatic DNL was inhibited by 82%.

Relative to chow feeding, Western diet feeding modestly reduced the fractional contribution of hepatic DNL by approximately 26%, likely resulting from the increased fat content of the diet relative to standard chow (Figure 4*A*). Chronic once-daily oral administration of PF-05221304 to Western diet–fed rats for 6 weeks produced dose-dependent reductions in hepatic DNL, relative to Western diet–fed vehicle rats. Treatment of Western diet–fed rats with 10 mg/kg PF-05221304 inhibited hepatic DNL by approximately 73% ($P < .0001$). Treatment with 1 or 3 mg/kg inhibited hepatic DNL by approximately 47% and approximately 58%, respectively, compared with Western diet vehicle treatment ($P < .001$ and $P < .0001$, respectively) (Figure 4*A*).

Relative to chow-fed rats, Western diet–fed vehicle-treated rats showed an approximately 5.6-fold increase in hepatic TG accumulation (Figure 4*B*). Chronic administration of PF-05221304 to Western diet–fed rats produced dose-dependent reductions in hepatic triglyceride levels, with the 2 highest doses (3 and 10 mg/kg) reducing hepatic triglyceride levels by approximately 60%, relative to Western diet vehicle rats ($P < .0001$). Hepatic TG levels at these doses were comparable with levels observed in chow-fed, vehicle-treated rats. Treatment with 1 mg/kg significantly decreased hepatic triglyceride levels by approximately 32%, relative to Western diet vehicle rats ($P < .01$) (Figure 4*B*). Administration of PF-05221304 did not alter body weight (Figure 4*C*), fasting TG concentrations (Figure 4*D*), or fasting cholesterol (Figure 4*E*). Fasting free fatty acids tended to increase in Western diet–fed rats administered PF-05221304 (Figure 4*F*).

Consistent with previous studies showing that acute ACC inhibitor administration increases β-hydroxybutyrate,[13] administration of PF-05221304 for 2 weeks increased β-hydroxybutyrate relative to vehicle (Figure 5*C*). However, with longer durations of administration, the increase

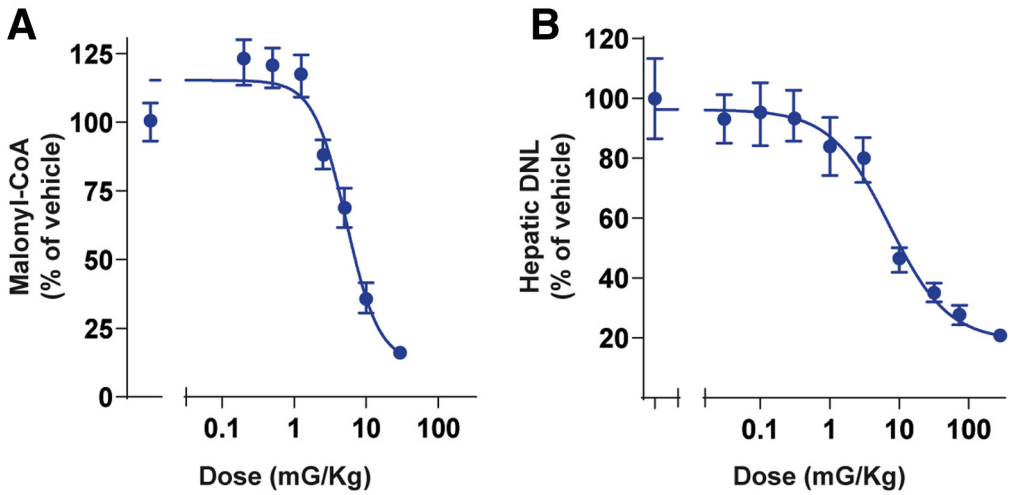

Figure 3. Effect of PF-05221304 on malonyl-CoA production, hepatic de novo lipogenesis, and steatosis in rats. (*A*) Acute oral administration of PF-05221304 inhibits hepatic malonyl-CoA levels in rats in a dose-dependent manner. n = 8 animals per treatment group. (*B*) Acute oral administration of PF-05221304 inhibits hepatic de novo lipogenesis, as assessed by ^{14}C-acetate incorporation into ^{14}C-labeled lipids, in a dose-dependent manner. n = 10 animals per treatment group.

in β-hydroxybutyrate was diminished. After 4 weeks of administration, fasting β-hydroxybutyrate levels were lower than in vehicle-treated animals, which likely is indicative of reduced liver fat content (Figure 4*G*). Fasting glucose levels (Figure 4*H*) were unchanged by PF-05221304 administration relative to Western diet–fed vehicle-treated rats. Similarly, the glucose/insulin ratio, a marker of insulin sensitivity, was not altered by PF-05221304 in the Western diet–fed rat (Figure 5*F*). Plasma TG, cholesterol, β hydroxybutyrate, free fatty acids, and glucose concentrations measured during the fed state at weeks 2, 3, and 4 are reported in Figure 5.

A poloxamer challenge was performed to assess the effects of PF-05221304 on very-low-density lipoprotein (VLDL)-TG secretion (Figure 4*I*). PF-05221304 showed higher TG levels over time relative to vehicle, but the slopes between the groups were roughly similar (5.3 mg/dL/min for ACC inhibitor and 4.9 mg/dL/min for vehicle).

PF-05221304 Inhibits Primary Human T-Cell Polarization to Proinflammatory Th17 Cells

Administration of PF-05221304 inhibited DNL with an IC_{50} of 23 nmol/L in primary human CD4+ CD45RA+ T cells cultured under conditions to drive Th17 polarization (Figure 6*A*). PF-05221304 produced a concentration-dependent suppression of interleukin (IL)17 secretion (IC_{50} of 151 nmol/L) (Figure 6*B*), reduced the quantity of IL17A+, CD4+ T cells assessed by flow cytometry (IC_{50} of 304 nmol/L) (Figure 6*C* and *D*), and reduced expression of the TH17 marker genes *IL-17A* (Figure 6*E*) and RAR-related orphan receptor C gene (Figure 6*F*), indicating suppressed polarization to proinflammatory Th17 cells. The reduction in IL17 secretion and IL17 expression is thought to be secondary to reduced numbers of TH17 cells because PF-05221304 blocked polarization of primary human CD4+ CD45RA+ T cells to IL17A+, CD4+ TH17 cells assessed by flow cytometry. In contrast, there was no change in expression of Treg marker *FoxP3* (Figure 6*G*), suggesting that polarization to the anti-inflammatory Treg cell type was not suppressed. These observations are consistent with previously published results showing that ACC inhibition blocks polarization of T cells to the proinflammatory TH17 T cells but not to anti-inflammatory Treg cells because DNL is essential for TH17 cell formation but not Treg formation.[10]

Chronic Administration of PF-05221304 Reduces Hepatic Inflammation in Diethylnitrosamine-Treated Rats

Administration of diethylnitrosamine (DEN) to rats produced a 58% suppression of hepatic TG relative to control rats (Figure 7*A*). Administration of PF-05221304 to rats that received DEN did not change hepatic TG levels relative to rats that received DEN and were treated with vehicle. Relative to control rats, administration of DEN increased the hepatic cluster of differentiation 3 (CD3) immunohistochemistry (IHC) staining area, a T-cell marker, from 0.20% to 0.55% (Figure 7*B*). Treatment with PF-05221304 in rats that received DEN decreased the average CD3 IHC staining area by 33% ($P < .05$). Similarly, relative to control rats, DEN administration produced an increase in hepatic α-smooth muscle actin (αSMA) IHC staining area, a marker for hepatic stellate cell activation and fibrogenesis, from 0.27% to 4.2% (Figure 7*C*). PF-05221304 reduced average αSMA IHC staining in animals that received DEN by 36% ($P < .05$). PF-05221304 administration showed a trend toward improvements in alanine aminotransferase (ALT) levels (Figure 7*D*), although this did not reach significance. Representative liver sections stained for CD3 and αSMA immunohistochemistry are shown (Figure 7*E*).

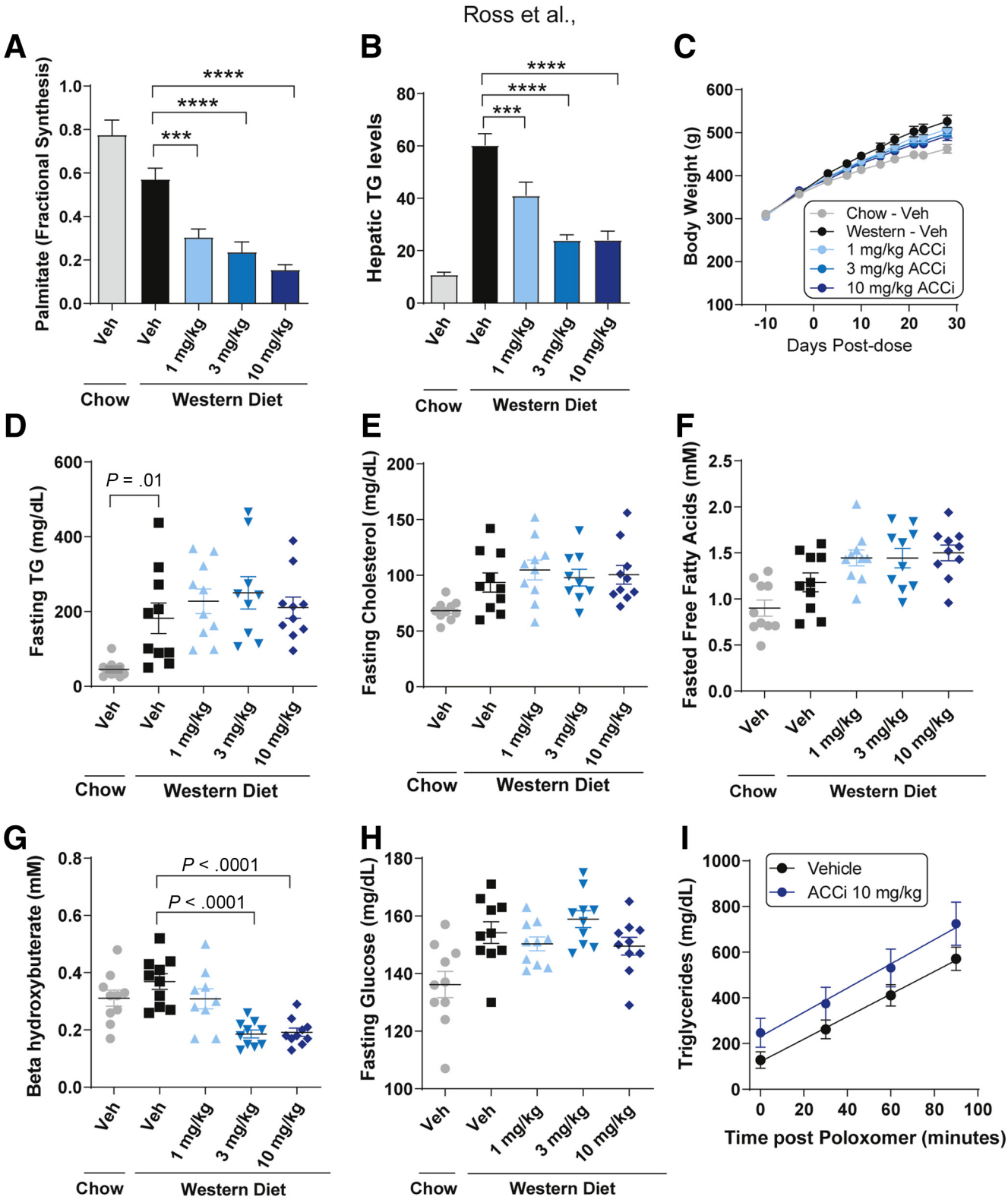

Figure 4. Effect of PF-05221304 on fractional hepatic de novo lipogenesis, steatosis, and metabolic parameters in Western diet–fed rats. (*A* and *B*) Once-daily oral administration of PF-05221304 for 4 weeks (*A*) suppresses hepatic DNL as assessed by deuterated water incorporation into lipids and (*B*) ameliorates hepatic steatosis in a dose-dependent manner. (*C*) Body weight, (*D*) fasting plasma TG, (*E*) cholesterol, (*F*) free fatty acids, (*G*) β hydroxybutyrate, and (*H*) glucose are shown. n = 10 animals per treatment group. (*I*) A poloxamer challenge was performed on a parallel cohort of animals to assess effects on hepatic VLDL-TG secretion. n = 6–8 per group. ***$P < .001$ relative to vehicle. ****$P < .0001$ relative to vehicle. ACCi, PF-05221304; Veh, vehicle.

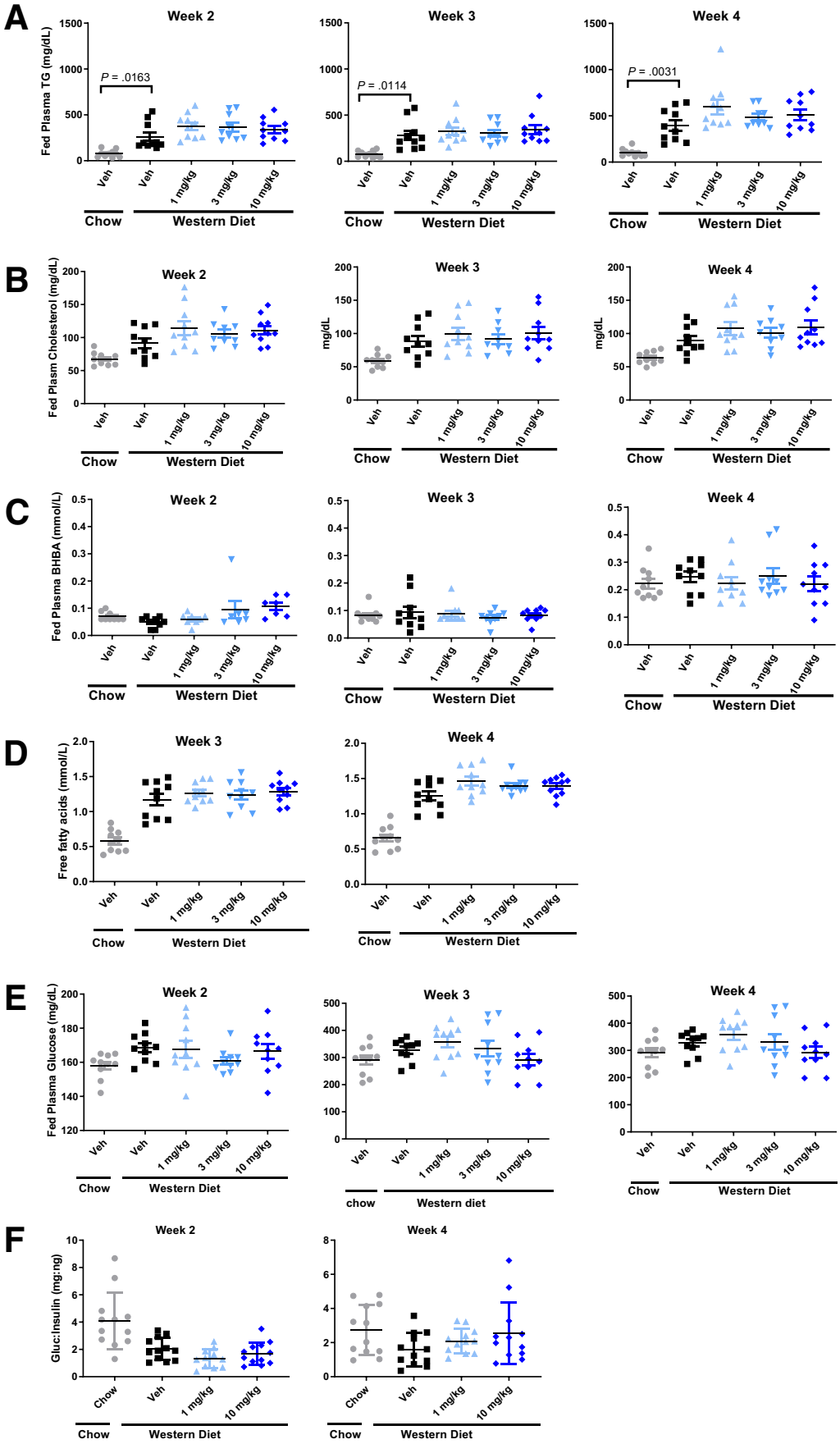
A
Week 2
Week 3
Week 4
Fed Plasma TG (mg/dL)
P = .0163
P = .0114
P = .0031
B
Fed Plasm Cholesterol (mg/dL)
C
Fed Plasma BHBA (mmol/L)
D
Free fatty acids (mmol/L)
E
Fed Plasma Glucose (mg/dL)
F
Gluc:Insulin (mg:ng)
Veh
1 mg/kg
3 mg/kg
10 mg/kg
Chow
Western Diet
chow
Western diet

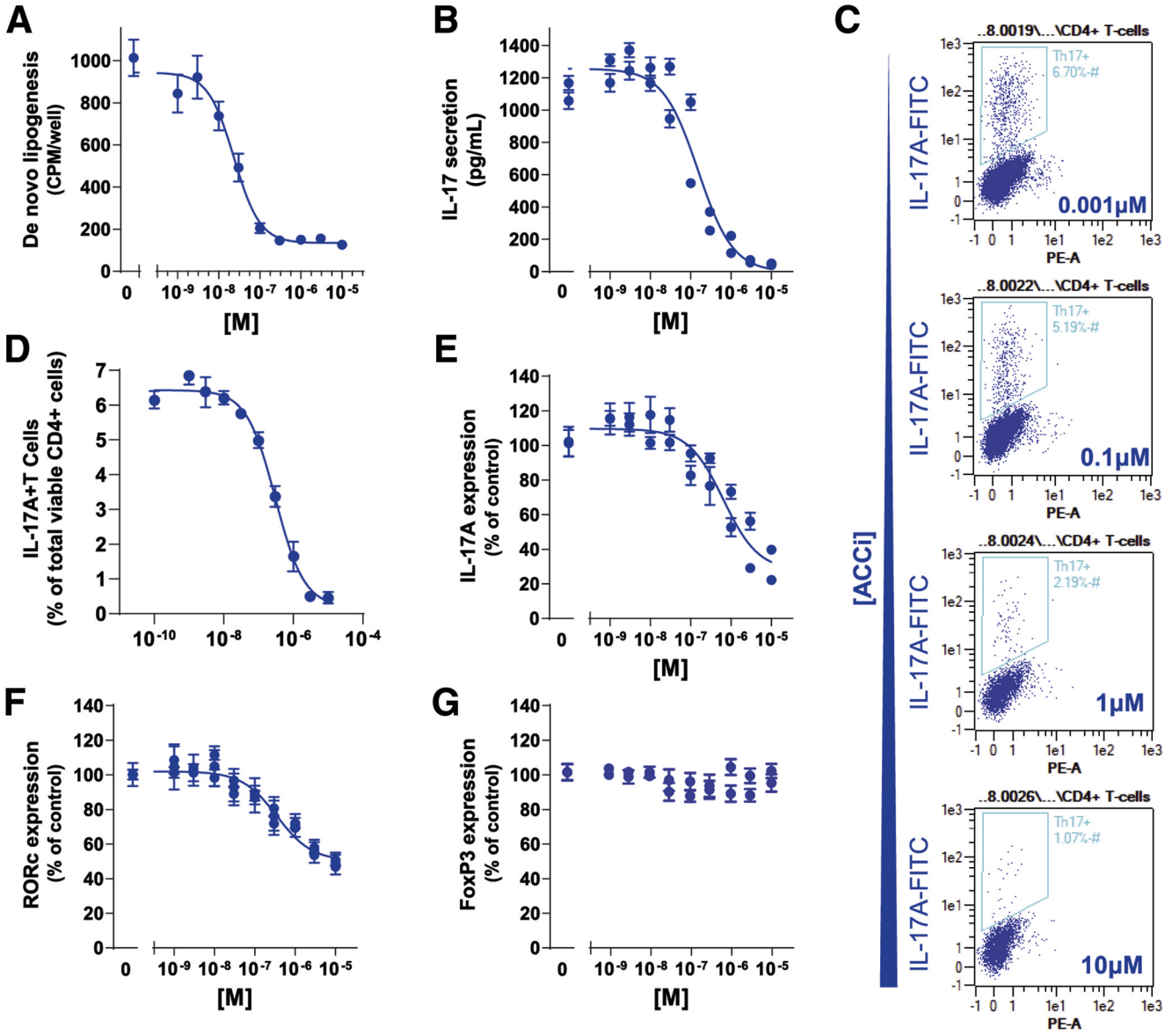

Figure 6. The effect of PF-05221304 on de novo lipogenesis primary human T cells and polarization to proinflammatory TH17 cells. (*A*) Effect of PF-05221304 on DNL in inflammatory human IL17 secreting T cells. (*B*) Effect of PF-05221304 on IL17 secretion, a specific marker for proinflammatory Th17 cells. (*C* and *D*) Effect of PF-05221304 on IL17A+ T cells expressed as a percentage of total CD4+ viable cells. (*E–G*) Effect of PF-05221304 on expression of (*E*) IL17A and (*F*) RAR-related orphan receptor C gene, markers for proinflammatory Th17 cells, and (*G*) FoxP3, a marker for anti-inflammatory Treg cells. n = 8 replicates from 2 independent experiments. FITC, fluorescein isothiocyanate.

PF-05221304 Suppresses Primary Human Stellate Cell Activation

Primary hepatic stellate cells (HSCs) treated with transforming growth factor $\beta 1$ (TGF$\beta 1$) over 72 hours resulted in transition of the HSC into an activated state as indicated by increased expression of both collagen and αSMA, and increased stellate cell proliferation relative to unstimulated control stellate cells. Consistent with effects in hepatocytes, PF-05221304 suppressed DNL in hepatic stellate cells with a median effective concentration (EC_{50}) of 31

Figure 5. (***See previous page***). **Circulating lipids and glucose in the fed state from the Western diet study.** (*A*) Plasma triglycerides, (*B*) cholesterol, (*C*) β hydroxybutyrate, (*D*) free fatty acids, and (E) glucose measured in the fed state from the Western diet study over time. Free fatty acids were not assessed at 2 weeks because of a technical error. (*F*) The glucose/insulin ratio was measured in a parallel study at weeks 2 and 4. n = 6–8 per group. BHBA, beta-hydroxybutyrate; Gluc, glucose; Veh, vehicle.

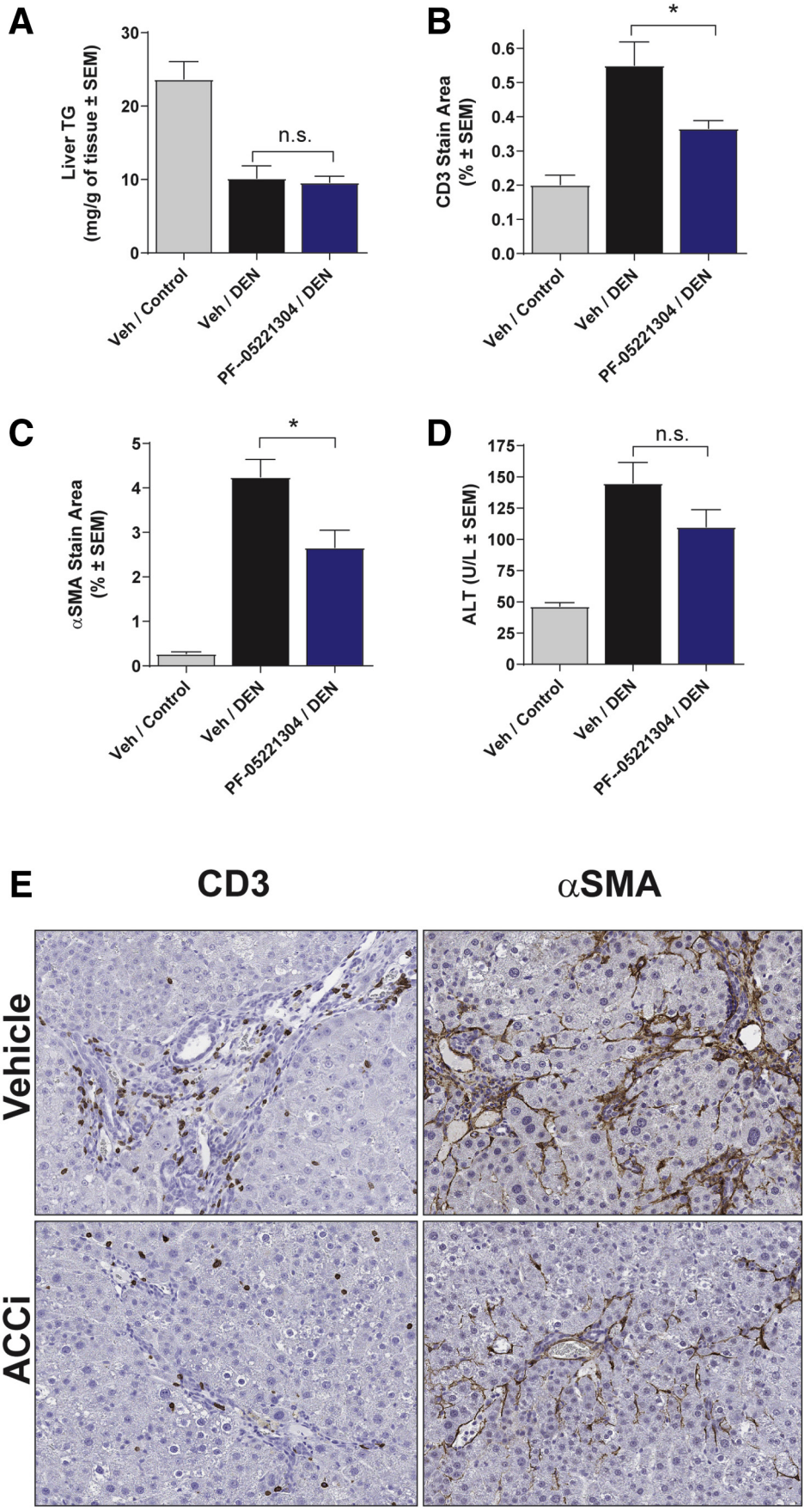

Figure 7. Effects of PF-05221304 on markers of inflammation and fibrogenesis in the DEN-induced hepatic inflammation model. (*A*) PF-05221304 does not alter liver triglycerides relative to vehicle in DEN-treated rats. (*B* and *C*) Effect of PF-05221304 administration on (*B*) CD3 and (*C*) αSMA immunohistochemistry staining. (*D* and *F*) Effect of PF-05221304 administration on (*D*) ALT levels and (*F*) liver weights. Representative histology images are shown for CD3 and αSMA immunohistochemistry. n = 10 animals per treatment group. *$P < .05$ relative to vehicle. ACCi, PF-05221304; Veh, vehicle.

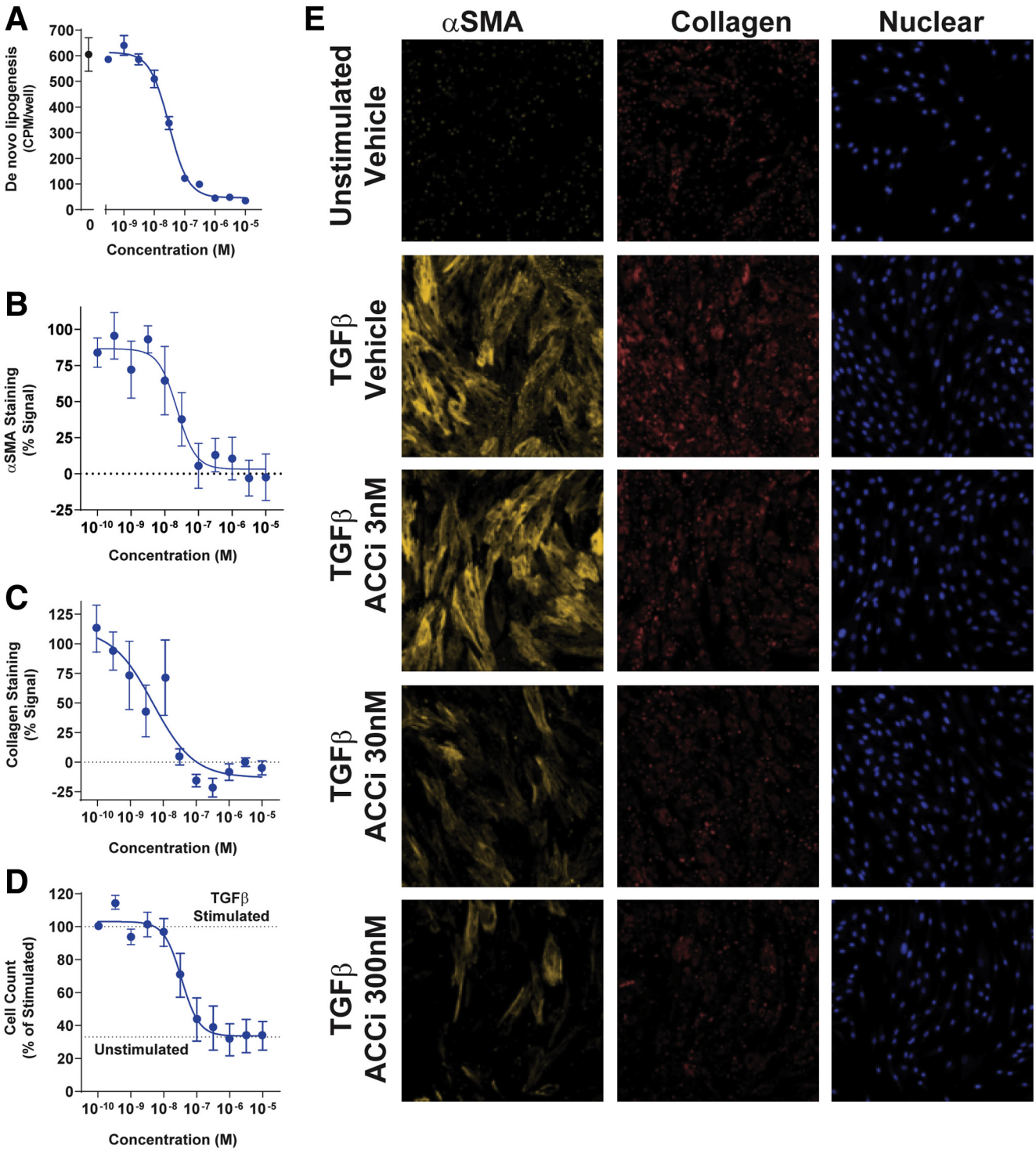

Figure 8. Effect of PF-05221304 on primary human stellate cell activation in vitro. (*A*) Concentration response curve of PF-05221304 inhibition of DNL. (*B* and *C*) Concentration response curves of PF-05221304 for markers of (*B*) stellate cell activation αSMA and (*C*) collagen staining. (*D*) Effects of PF-05221304 on TGFβ1-induced stellate cell proliferation. Cell number in TGFβ1-stimulated and unstimulated control wells are indicted by *dashed horizontal lines*. (*E*) Images of αSMA, collagen, and nuclear cell count staining showing signal from unstimulated, TGFβ1-stimulated vehicle-treated cells, and TGFβ1-stimulated cells treated with 3 nmol/L, 30 nmol/L, and 300 nmol/L PF-05221304. ACCi, PF-05221304.

nmol/L (Figure 8*A*). PF-05221304 dose-dependently and robustly attenuated myofibroblast activation, with potent inhibition of both collagen (Figure 8*C* and *E*) and αSMA (Figure 8*B* and *E*) induction with an EC_{50} of 5 nmol/L and 23 nmol/L, respectively. In addition, PF-05221304 was found to block TGFβ1-induced stellate cell proliferation,

normalizing the cell count to levels observed in the unstimulated control wells (Figure 8*D* and *E*).

Chronic Administration of PF-05221304 Reduces Hepatic Inflammation and Fibrosis in Choline-Deficient and High-Fat Diet–Fed Rats

Relative to chow-fed rats, rats fed the choline-deficient and high-fat diet (CDAHFD) showed a marked progressive increase in liver stiffness over the duration of the study (Figure 9*A*), indicative of increased hepatic inflammation and fibrosis. From the baseline (defined as the measurement made just before initiation of vehicle or PF-05221304 administration), liver stiffness increased by 4.7 kPa by week 3 and by 9.7 kPa by week 6. Administration of PF-05221304 blunted the progression of liver stiffness from baseline at these time points by 67% and 66%, respectively, relative to vehicle-administered CDAHFD rats. This resulted in a reduction in liver stiffness of 23% ($P < .01$) at week 4 and 35% ($P < .001$) at week 6 relative to vehicle-treated rats.

ALT (Figure 9*B*) and aspartate aminotransferase (AST) (Figure 9*C*) levels were increased in vehicle-treated CDAHFD-fed rats relative to chow-fed rats, reaching a maximum at week 3, but decreasing from this peak at week 6, likely reflective of more advanced liver damage.[14] Relative to vehicle administration, administration of PF-05221304 significantly reduced the week 3 peak ALT (Figure 9*B*) and AST (Figure 9*C*) levels in CDAHFD-fed rats by 37% ($P < .01$) and 24% ($P < .05$), respectively, although this effect did not persist to week 6 when ALT and AST levels were below or at baseline levels. Relative to chow-fed rats, CDAHFD-fed rats administered vehicle showed an 11-fold increase in hepatic triglyceride accumulation (Figure 9*D*). Chronic administration of PF-05221304 did not significantly alter hepatic TG accumulation, relative to CDAHFD-fed rats that were administered vehicle. Relative to chow-fed control rats, CDAHFD-fed rats treated with vehicle showed a 22-fold increase in αSMA staining area (Figure 9*E* and *G*). Administration of PF-05221304 reduced this by 41% ($P < .01$) relative to vehicle-treated CDAHFD-fed rats. Similarly, Picro Sirius red (PSR) staining was increased by 7.9-fold in vehicle-treated CDAHFD-fed rats reactive to control rats fed a chow diet (Figure 9*F* and *G*). The PSR staining area was reduced by 26% ($P < .05$) in CDAHFD-fed rats treated with PF-05221304 relative to vehicle-treated CDAHFD-fed rats. Representative histology data for H&E, oil red O, αSMA, and PSR are shown in Figure 9*G*. Body weight, plasma triglycerides, cholesterol, free fatty acids, β hydroxybutyrate, and glucose levels were not altered in CDAHFD-fed rats administered PF-05221304, relative to rats administered vehicle (Figure 10). Relative to chow-fed control rats, CDAHFD-fed rats administered vehicle showed a marked increase in hepatic expression of the activated myofibroblast marker *α-SMA* (Figure 11*A*), and the fibrosis marker genes *Col1A1* (Figure 11*B*) and *Col3A1* (Figure 11*C*). Administration of PF-05221304 reduced expression of these genes by 46% ($P < .01$), 40% ($P < .01$), and 44% ($P < .05$), respectively, indicative of a reduction in hepatic fibrotic tone. In addition, the hepatic expression of multiple inflammatory markers was increased in CDAHFD-fed rats administered vehicle (Figures 11*D* and *E* and 12). Administration of PF-05221304 reduced the hepatic expression of a subset of these markers including *CCL2* (Figure 11*D*) and *CCL11* (Figure 11*E*), which were reduced by 61% ($P < .001$) and 45% ($P < .05$), respectively. Consistent with the reduced hepatic expression of *CCL2*, circulating CCL2 levels were reduced 23% ($P < .05$) by administration of PF-05221304 (Figure 11*F*).

Discussion

In the present studies, the dual ACC1/2 inhibitor PF-05221304 was shown to exert efficacy on multiple dimensions of NASH pathogenesis. PF-05221304 inhibited DNL, stimulated fatty acid oxidation, and reduced TG accumulation in primary human hepatocytes. Similarly, PF-05221304 inhibited hepatic DNL in single oral dose studies in lean rats and in chronic studies in Western diet–fed rats, PF-05221304 inhibited DNL and normalized steatosis. ACC inhibition has been shown previously to inhibit DNL and reduce steatosis in rodents[8,9] and in human beings.[15,16] However, increased circulating TG levels and free fatty acids have been reported to be a mechanistic consequence of hepatic ACC inhibition owing to compensatory increases in sterol regulatory element-binding protein activation.[15] Kim et al[15] reported approximately 2- to 3-fold increases in circulating TG and free fatty acid levels in hepatic ACC knockout mice as a consequence of compensatory activation of sterol regulatory element-binding protein leading to increased lipid secretion from the liver. Furthermore, reductions in TG clearance also have been reported to contribute to increased circulating lipids in response to ACC inhibition.[13] In the present study, increases in fasted or fed circulating TG levels of this magnitude were not observed at the doses evaluated, although trends toward increases in fed-state plasma TGs and fasted- and fed-state free fatty acids were observed. One hypothesis is that differences in the magnitude of DNL inhibition between the present study and the study by Kim et al[15] contributed to this difference. The present studies used doses that only partially suppressed hepatic DNL (≤70% inhibition), whereas Kim et al[16] evaluated doses that fully ablated hepatic DNL and hepatic ACC knockout mice. These observations suggest that doses that only partially suppress DNL, rather than ablate DNL activity, may be sufficient to reduce hepatic steatosis, but not sufficient to induce 2- to 3-fold increases in circulating TG levels. Consistent with these hypotheses, circulating TG increases were observed to be dose-responsive to PF-05221304 in both healthy subjects[12] and in patients with NAFLD,[17] although the dose response was left-shifted and more pronounced at lower doses in NAFLD patients than in healthy subjects.

To assess the effects of PF-05221304 on hepatic VLDL-TG secretion, a poloxamer challenge was conducted in the Western diet model. PF-05221304 increased baseline circulating TG levels relative to vehicle in the poloxamer challenge, but the slopes were roughly similar between the treatment groups, suggesting no difference in VLDL-TG

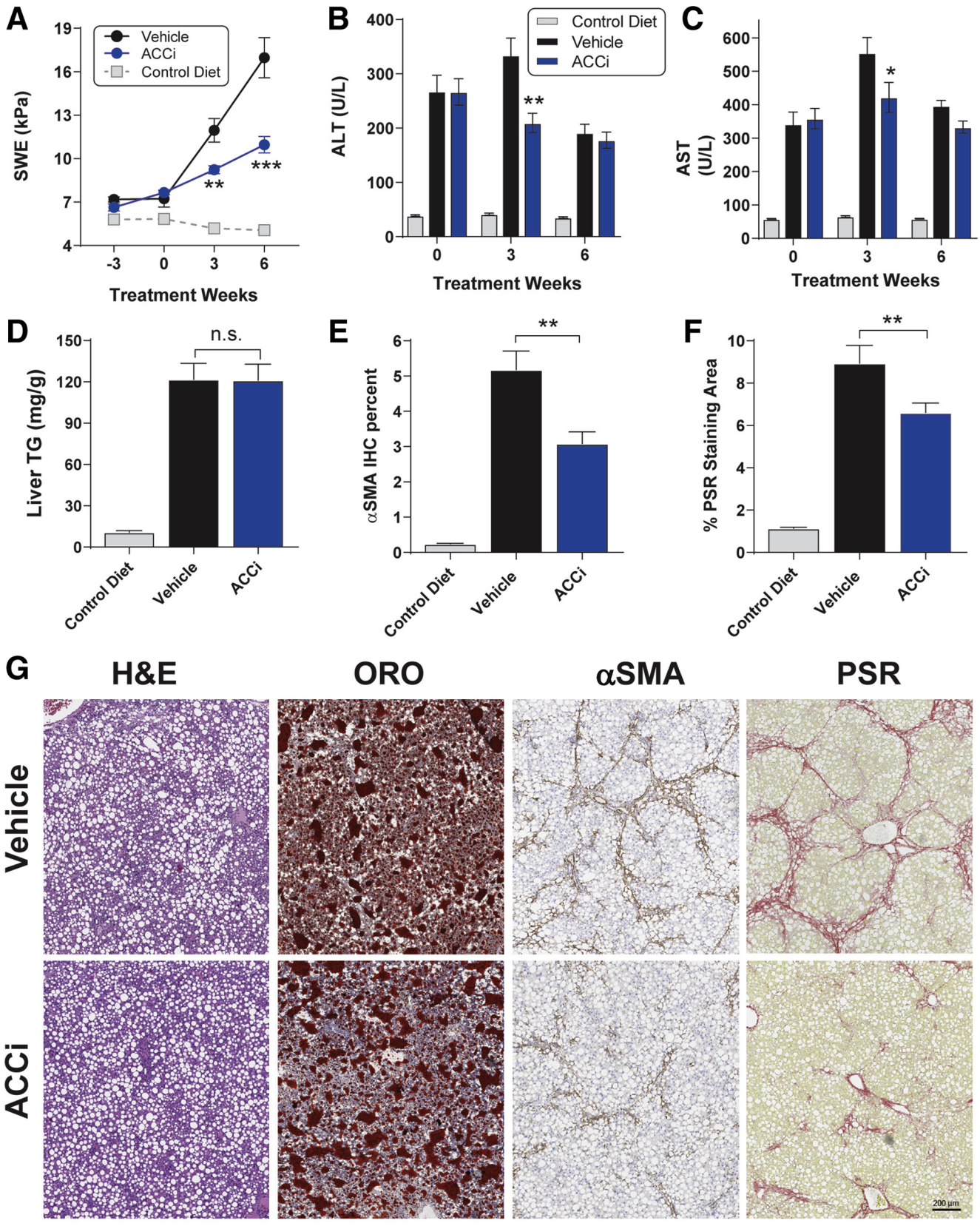

Figure 9. Effect of PF-05221304 vs vehicle in the choline-deficient high-fat diet model. (*A*) Administration of PF-05221304 decreases liver stiffness as assessed by SWE. (*B*) ALT and (*C*) AST levels over time. (*D*) PF-05221304 administration does not alter steatosis relative to vehicle administration in the CDAHFD model. (*E*) PF-05221304 reduces αSMA immunohistochemistry staining. (*F*) PF-05221034 reduces picrosirius red staining area. (*G*) Representative histology images for H&E staining, oil red O staining, αSMA immunohistochemistry, and PSR staining are shown. (*E* and *F*) Images shown are from the animal with a median response in the image analysis. N = 12 animals per treatment group. *$P < .05$ relative to vehicle. **$P < .01$ relative to vehicle. ***$P < .001$ relative to vehicle. ACCi, PF-05221304; ORO, oil red O.

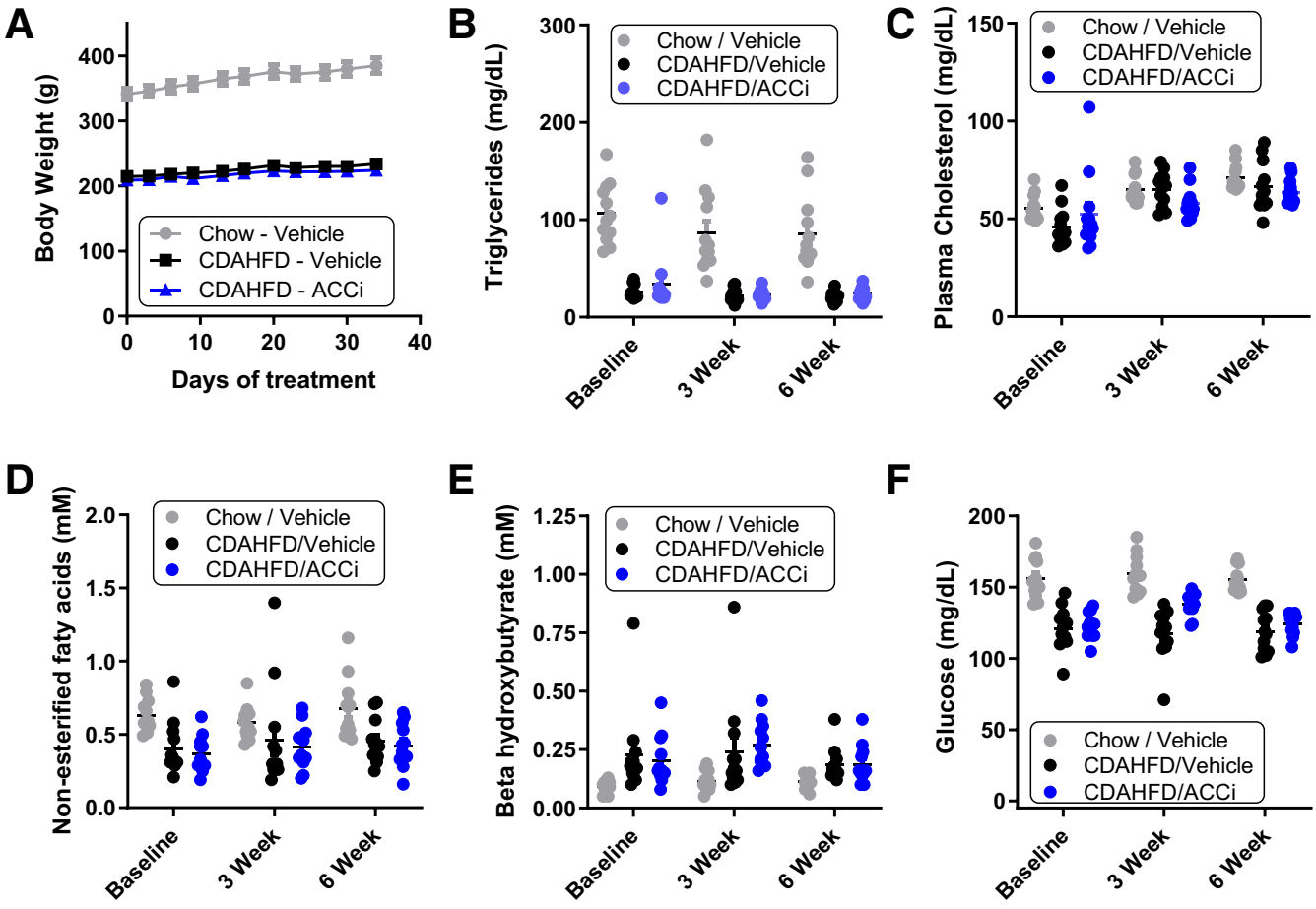

Figure 10. Body weight, circulating lipids, and glucose in the fed state from the CDAHFD study. (*A*) Body weight, (*B*) plasma triglycerides, (*C*) cholesterol, (*D*) β hydroxybutyrate, (*E*) free fatty acids, and (*F*) glucose measured in the fed state from the Western diet study over time. N = 12 animals per treatment group. ACCi, PF-05221304.

secretion rates during the poloxamer challenge in this study. Previous studies have shown that both decreased TG clearance[13] and increased VLDL-TG secretion[13,15] contribute to ACC inhibitor-induced TG increases in other model systems. The reasons why an increase in VLDL-TG secretion was not observed in the present study are not entirely clear, however, as noted earlier, the prior studies also showed more marked TG increases than observed with the doses of PF-05221304 used in the present work.

In the present studies, PF-05221304 was weight neutral. This is not surprising because increases in fatty acid oxidation in the absence of increased energy expenditure do not alter body weight or fat mass.[18] ACC inhibition has been shown to increase fatty acid oxidation (as assessed by respiratory quotient using indirect calorimetry) but not increase energy expenditure (as measured by oxygen consumption per unit of time using indirect calorimetry) in rodents and human subjects.[19] PF-05221304 is expected to have a less-pronounced effect on whole-body fuel substrate utilization because the compound is liver targeted.[12]

The effects of ACC inhibitors on glycemic control is controversial, with some studies showing improvements in insulin sensitivity[9,13,20,21] and others not.[15,22] In the present studies, PF-05221304 had no clear effects on fasting glucose level or the glucose/insulin ratio in Western diet–fed rats. Conversely, PF-05221304 produced dose-dependent and significant reductions in hemoglobin A1c in NAFLD patients with more pronounced reductions observed in the subset of patients with type 2 diabetes mellitus.[17] The reasons for these differences are not clear, but the window for detection of glycemic improvement in the Western diet–fed rat model may have been suboptimal because the animals were neither overtly diabetic nor had pronounced insulin resistance.

The present study also investigated the direct effect of PF-05221304 on aspects of the inflammatory and fibrotic components of NASH pathogenesis in model systems. The inflammatory response in NASH is complex, involving infiltration of multiple immune cell types such as monocytes, T lymphocytes, and neutrophils, as well as activation and expansion of liver resident cells including hepatic stellate cells.[23] Progression from simple steatosis to NASH in human subjects is characterized by a higher frequency of hepatic proinflammatory TH17 cells and an increase in the ratio of proinflammatory TH17 cells to anti-inflammatory Treg cells in circulation,[10] and this shift was hypothesized to

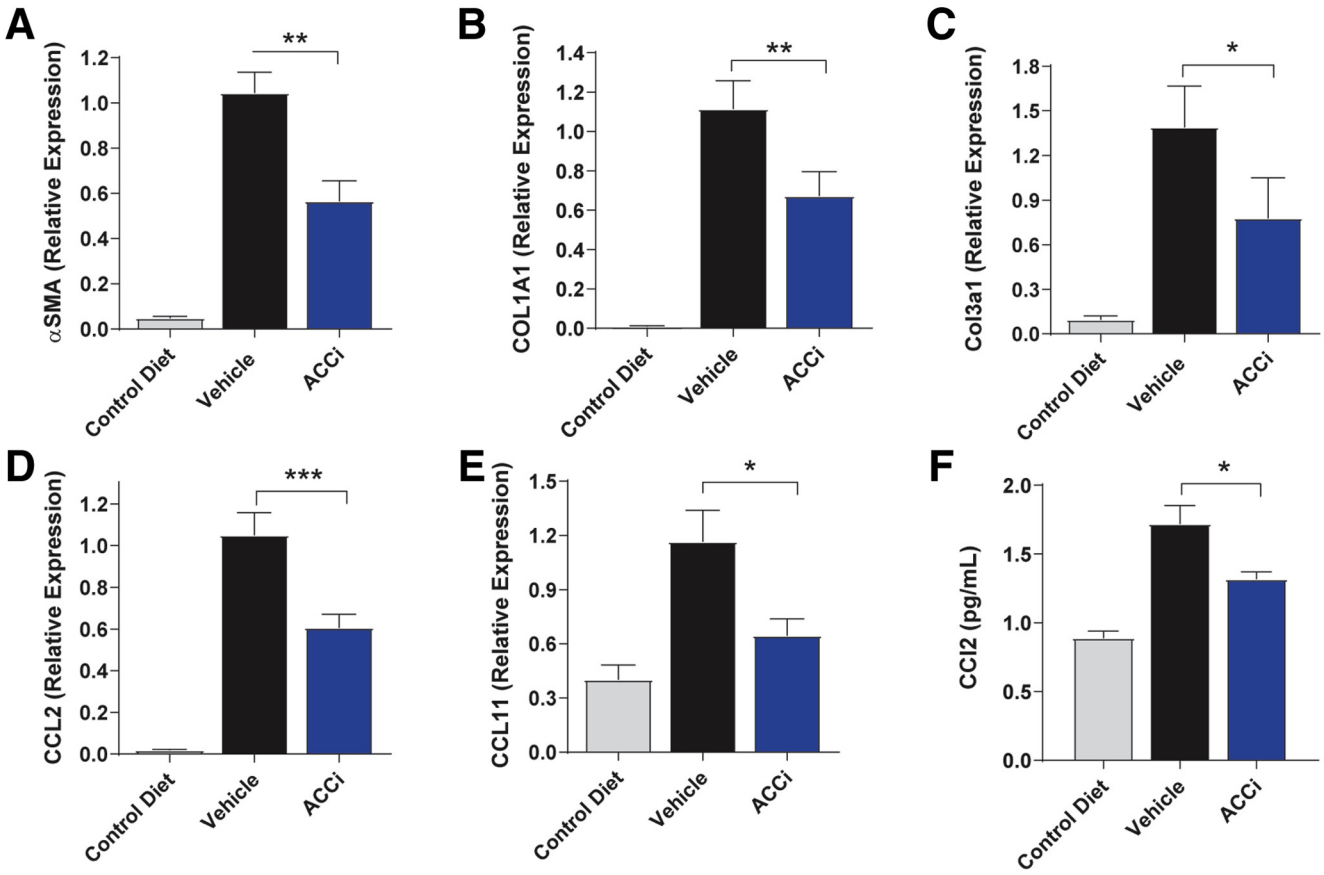

Figure 11. Effect of PF-05221304 vs vehicle in hepatic gene expression and circulating CCL2 in the choline-deficient high-fat diet model. (*A–F*) Hepatic expression of (*A*) αSMA, (*B*) COL1A1 (*C*) COL3A1, (*D*) C-C motif chemokine ligand 2, and (*E*) C-C motif chemokine ligand 11 are shown. (*F*) Circulating C-C motif chemokine ligand 2 levels are reported. N = 12 animals per treatment group. *$P < .05$ relative to vehicle. **$P < .01$ relative to vehicle. ***$P < .001$ relative to vehicle. ACCi, PF-05221304.

contribute to the progression from simple steatosis to NASH.[24,25] T cells undergo metabolic shift during activation[26]; mammalian target of rapamycin and hypoxia-inducible factor 1α play a critical role in polarizing T cells toward the proinflammatory TH17 subtype by promoting glycolysis and lipogenesis.[27] Conversely, activation of 5′ adenosine monophosphate-activated protein kinase, which suppresses lipogenesis, opposes mammalian target of rapamycin, promotes fatty acid oxidation rather than glycolysis, and promotes polarization to the anti-inflammatory Treg cells.[28] Berod et al[10] showed that inhibition of DNL flux by suppression of ACC activity blocks polarization of T cells to proinflammatory TH17 cells, but not anti-inflammatory Treg cells. Consistent with this, PF-05221304 was found to suppress DNL in undifferentiated primary human T cells and to block polarization of these cells to proinflammatory TH17 cells as assessed by quantification of IL17A+, CD4+ cells by flow cytometry, IL17 secretion, and expression of the specific TH17 cell markers IL17A and RAR-related orphan receptor C gene. In contrast, polarization to anti-inflammatory Treg cells, as evidenced by expression of the Treg-specific marker FoxP3, was not altered.

PF-05221304 also was shown to inhibit DNL in, and block activation of primary human HSCs toward, formation of myofibroblasts as assessed by αSMA immunohistochemistry, collagen staining, and myofibroblast proliferation. Activation of HSCs into myofibroblasts is recognized as a key driver of fibrosis in response to hepatic injury,[29] and blockade of HSC activation and proliferation may be an attractive strategy to reduce fibrosis. The process governing the transition from quiescent HSCs to activated myofibroblasts is complex, involving both signaling and metabolic adaptations. The specific mechanism by which PF-05221304 blocks HSC activation is presently unknown, but other ACC inhibitors also were shown to block HSC activation, suggesting this effect is a consequence of ACC inhibition and suppression of DNL. Inhibition of myofibroblast proliferation may have contributed in part to suppressed myofibroblast activation. Consistent with this, ACC inhibitors also have been shown to reduce proliferation of other highly proliferative cells such as T cells[10] and some tumor cell types.[30–33] Inhibition of proliferation alone, however, is unlikely to account for the effects of PF-05221034 because inhibition of HSC activation as assessed by collagen staining was observed at lower doses (EC_{50} = 5 nmol/L) than those that suppressed HSC proliferation (EC_{50} = 35 nmol/L). ACC inhibitors also have been shown to

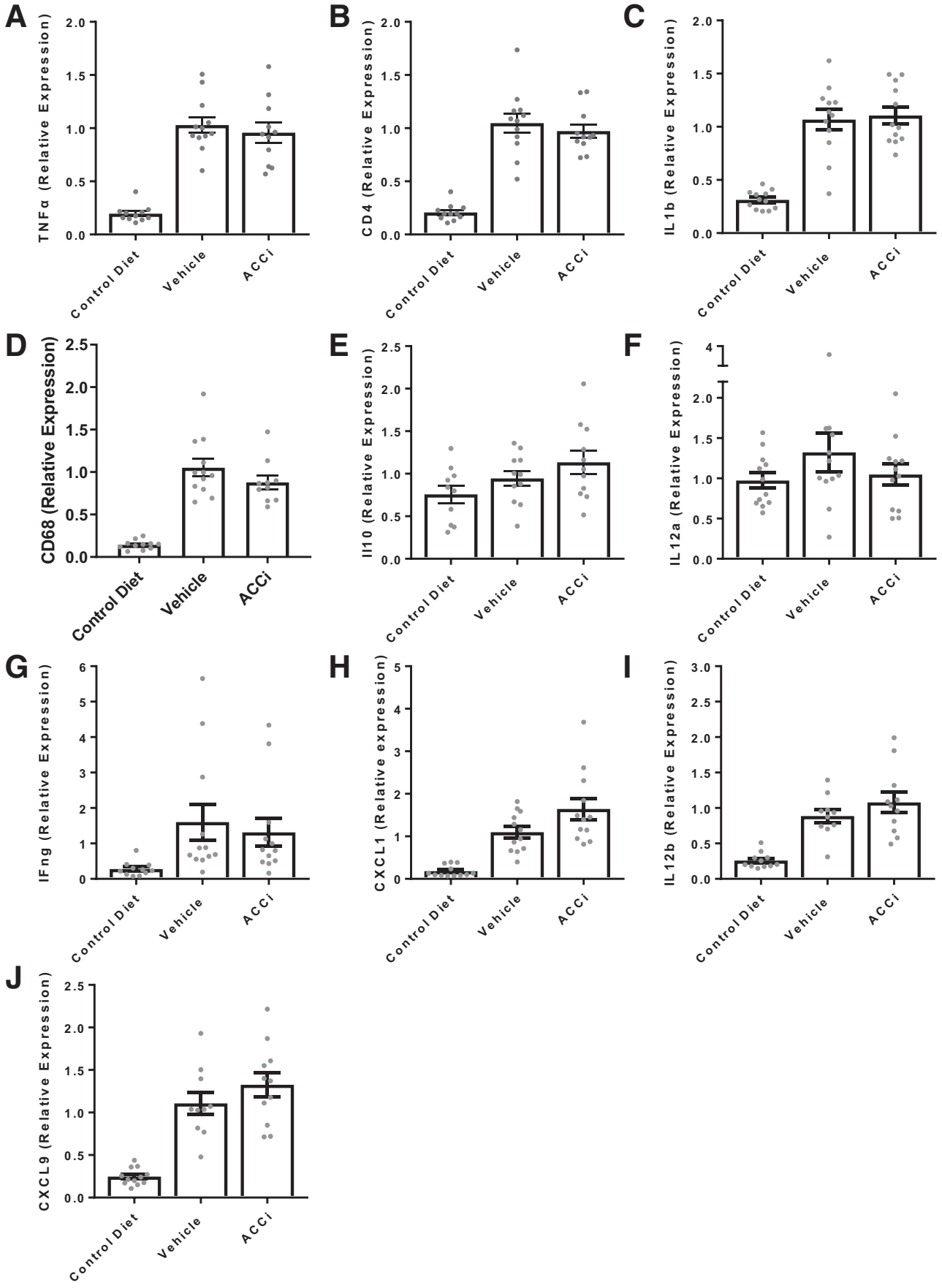
A
TNFα (Relative Expression)
B
CD4 (Relative Expression)
C
IL1b (Relative Expression)
D
CD68 (Relative Expression)
E
Il10 (Relative Expression)
F
IL12a (Relative Expression)
G
IFng (Relative Expression)
H
CXCL1 (Relative expression)
I
IL12b (Relative Expression)
J
CXCL9 (Relative Expression)
Control Diet
Vehicle
ACCi

modulate Wnt and Hedgehog signaling in some systems,[34] both of which contribute to HSC activation.[29] Additional studies are needed to determine the precise molecular mechanism underlying the effects of ACC inhibition on HSC activation.

Consistent with these observations, PF-05221304 reduced markers of hepatic inflammation and fibrogenesis in the DEN-induced liver injury and the CDAHFD models. The DEN model, which is a chemical-induced liver injury model, was selected to probe the direct effects of PF-05221304 on hepatic inflammation and fibrogenesis, independent of any benefits that could be realized from reduced lipotoxicity in NASH. Administration of DEN decreases levels of liver fat to less than those observed in control chow-fed animals and further reductions were not observed in animals that received daily administration of PF-05221304. Similarly, choline deficiency coupled with administration of a high-fat diet lead to pronounced steatosis as a result of lipid loading and impairment in clearance of lipid from the liver; liver fat levels were not altered by PF-05221304 in this model. Liver fat accumulation in the CDAHFD model is driven by choline deficiency, which is a nonphysiological condition that prevents TG export from the liver, coupled with artificially high dietary fat content. Because liver fat accumulation in this model is not driven by increased DNL flux (which drives steatosis in patients with NAFLD[4]), but rather is a consequence of choline deficiency, an ACC inhibitor would not be expected to reduce steatosis in this model. Rather, the goal of evaluating PF-05221304 in the CDAHFD model, similar to the DEN model, was specifically to investigate if ACC inhibition could lead directly to improvements in hepatic inflammation and fibrosis in the absence of changes in steatosis. The observation that the ACC inhibitor did not reduce steatosis in the CDAHFD model (in which steatosis is driven by artificial means) does not suggest that the molecule does not act to reduce steatosis. Indeed, PF-05221304 produced robust reductions in steatosis in the Western diet model (in which increased DNL flux contributes to steatosis as was observed in NAFLD patients) and produced pronounced reductions in steatosis in patients with NAFLD or NASH.[17] Rather, the observations that improvements in fibrosis and inflammation were observed despite no changes in steatosis suggest that there are benefits to ACC inhibition beyond steatosis reductions. These observations are consistent with the direct effects of the molecule on inhibition of hepatic stellate cell activation and polarization of T cells to proinflammatory TH17 cells. Thus, the observed improvements in inflammation and fibrosis makers in these models likely reflect a direct benefit on these pathways rather than downstream benefits of improvements in steatosis and lipotoxicity. Although effects on steatosis were not observed in either of these models, we cannot exclude the possibility that PF-05221304 blocked formation of DNL-derived lipotoxic intermediates in the CDAHFD model, and that this contributed to the observed antifibrogenic benefits.

The results presented here provide experimental evidence that liver-directed dual-ACC1/2 inhibitor PF-05221304 produces improvements in multiple dimensions of NASH pathogenesis including reduced hepatic lipid accumulation, suppressed hepatic inflammation, and inhibition of hepatic fibrogenesis. Additional studies to assess the effectiveness of PF-05221304 in NASH patients are needed to evaluate the human translation of these findings. The results of the nonclinical studies reported here support that such studies are warranted.

Methods and Materials

All authors had access to the study data and reviewed and approved the final manuscript. All procedures performed on animals were in accordance with regulations and established guidelines and were reviewed and approved by an Institutional Animal Care and Use Committee or through an ethical review process.

Enzymology

Inhibition assay. PF-05221304 was evaluated for dose-responsive inhibition of rat and human ACC1 and ACC2. PF-05221304 was pre-incubated with 37°C/citrate-activated ACC enzyme (0.6 μg/mL) before initiating the reaction with the addition of substrate solution (containing 2.4 mmol/L acetyl-CoA, 38.4 mmol/L $KHCO_3$, 1.6 mmol/L NaH $[^{14}C]O_3$, and 8.0 mmol/L ATP). After 20 minutes, the reaction was terminated by the addition of HCl, with the concomitant liberation of nonreacted $NaHCO_3$ as CO_2. The plates were dried overnight to allow complete $[^{14}C]O_2$ liberation. The reaction product, [^{14}C]malonyl-CoA, was measured after the addition of OptiPhase (Perkin Elmer, Waltham, MA) Supermix liquid scintillation fluid using a Microbeta (Perkin Elmer) LSC luminescence counter. Data were analyzed by statistical methods (described later).

Reversibility assay. Reversibility was assessed by dilution. Reactions (1 uninhibited, 1 with 3 nmol/L compound, and 2 with 30 nmol/L compound) containing 5 μg/mL hACC1 were initiated by the addition of substrate. At each time point, an aliquot was removed to assess ^{14}C malonyl-CoA production as described earlier. At 6 minutes the reactions were diluted 10-fold. The uninhibited reaction was diluted with substrate, the 3 nmol/L reaction was diluted with substrate containing 3 nmol/L compound, and 1 of the 30 nmol/L reactions was diluted with substrate containing 30 nmol/L compound. The other 30 nmol/L reaction was diluted with substrate containing 3 nmol/L compound.

Inhibition kinetics. The mode of inhibition of hACC2 was examined using 3 different substrate conditions. In each

Figure 12. (***See previous page***). **Hepatic inflammatory gene expression from the choline-deficient and high-fat diet study—pathways that were not altered by ACC inhibition.** (*A*) TNFα; (*B*) CD4; (*C*) ILb; (*D*) CD68; (*E*) IL10; (*F*) IL12a; (*G*) interferon gamma; (*H*) chemokine (C-X-C motif) ligand 1; (*I*) IL12b; (*J*) CXCL9. N = 12 animals per treatment group. *Bars* represent the means ± SEM. *Symbols* represent individual values. ACCi, PF-05221304.

case, the concentration of activated hACC1 was 1.2 μg/mL. Reactions were initiated by the addition of substrate and terminated by addition of HCL after 15 minutes at room temperature.

To determine the mode of inhibition relative to ATP, the concentration of ATP in the reaction was varied from 25 to 1000 μmol/L with saturating concentrations of acetyl-CoA (600 μmol/L) and carbonate (9.6 mmol/L potassium bicarbonate and 0.4 mmol/L NaH[^{14}C]O_3 [58 mCi/mmol]).

To determine the mode of inhibition relative to acetyl-CoA, the concentration of acetyl-CoA was varied from 12.5 to 600 μmol/L in the presence of saturating concentrations of ATP and carbonate. To determine the mode of inhibition relative to carbonate, the concentration of total carbonate (0.23 mCi/mmol) was varied from 3.13 to 200 mmol/L with saturating ATP and acetyl-CoA.

Statistics. For dose-response experiments, the response was expressed as the ACC activity relative to the control (uninhibited level) treatment. The procedure NLMixed of the SAS (Cary, NC) system was used to fit the log–logistic function modeling the dose–response relationship and to take into account the variability observed for each experiment (random effect). Data are expressed as the mean estimate for the response at each dose and the 95% confidence bounds of these estimates.

Effect of PF-05221304 on De Novo Lipogenesis in Cryopreserved Primary Human Hepatocytes

Cryopreserved primary human hepatocytes (donor HH AA 508) obtained from BD Gentest (lot 318; San Jose, CA) were plated at 50,000 cells/well in a 96-well collagen-coated plate using Corning Cryo plating media. After a 4-hour incubation, plating media was replaced with Williams E maintenance media. On the following day, PF-05221304 was dissolved in dimethyl sulfoxide (DMSO), serially diluted, and added to the cells. After a 1-hour incubation with compound or vehicle, [^{14}C] acetate was added to each well and cells were incubated for 2 hours. Upon termination of the experiment, cells were lysed and the resulting cell lysate from each well was transferred to a 96-well, clear-bottomed isoplate and mixed with microscint-E (Perkin Elmer). [^{14}C]-labeled lipid was measured using a Microbeta (Perkin Elmer) scintillation counter.

Effect of PF-05221304 on Hepatic β-Oxidation in Cryopreserved Primary Human Hepatocytes

Cryopreserved primary human hepatocytes (donor HH AA 508) obtained from BD Gentest (lot 318) were plated at 50,000 cells/well in a 24-well, collagen-coated plate using Corning Cryo plating media. After a 1-hour preincubation, vehicle (0.1% DMSO) or PF-05221304 (10 μmol/L) was added to wells and incubated for an additional 30 minutes. A substrate solution containing 33 nmol/L [9,10-^{3}H]palmitic acid and 1 mmol/L carnitine was added and incubated for 2 hours. The reaction was terminated by addition of 10% (w/v) trichloroacetic acid, and the lipid fraction was removed by organic extraction with diethyl ether. The β-oxidation product ($^{3}H_2O$) was determined by evaporating the aqueous fraction to dryness and counting on a scintillation counter.

Effects of PF-05221304 on Triglyceride Accumulation in Cryopreserved Primary Human Hepatocytes

Cryopreserved primary human hepatocytes (donor HH AA 508) obtained from BD Gentest (lot 318) were plated at 350,000 cells/well in a 24-well, collagen-coated plate using Williams E maintenance media. After a 4-hour incubation, Williams E maintenance media was replaced with starvation media (1 g/L D-glucose Dulbecco's modified Eagle medium, 100 nmol/L dexamethasone, 100 nmol/L insulin, and 100 nmol/L penicillin/streptomycin). After a 2-hour incubation, starvation media was replaced with assay media (1 g/L D-glucose Dulbecco's modified Eagle medium, 100 nmol/L dexamethasone, 1× ITS+ media supplement and 1× penicillin/streptomycin; Corning, Corning, NY) supplemented with either 10 μmol/L PF-05221304 or 0.1% DMSO.

Cells were harvested for lipidomic analysis at 2 hours, 24 hours, and 48 hours after compound administration. Upon termination of the experiment, hepatocytes were lysed with methanol:water and lipids were isolated by organic extraction with dichloromethane:isopropanol:methanol (25:10:65, v/v/v). Lipid extracts then were analyzed by ultra performance liquid chromatography tandem mass spectrometry (MS).

Effects of Single Dose of PF-05221304 on Inhibition of Malonyl-CoA in Rats

Male Sprague–Dawley (~200 g) rats were double-housed under standard laboratory conditions and kept under a 12:12-hour light-dark schedule (lights on at 6:00 AM). Rats were weighed and dosed orally with a single administration of either vehicle control (0.5% methyl cellulose [MC]) or PF-05221304 ranging from 0.07 to 30 mg/kg. Two hours after the dose, the animals were killed by CO_2 asphyxiation. Blood was collected via cardiac puncture. Livers were rapidly removed and freeze-clamped and frozen livers were pulverized on a N_2 cooled aluminum block. Powdered liver was homogenized using lysing tubes containing 10% trichloroacetic acid. After centrifugation, the supernatant was removed and malonyl-CoA was analyzed by liquid chromatography MS.

Effects of Single Dose of PF-05221304 on Inhibition of De Novo Lipogenesis in Rats

Male Sprague–Dawley (~200 g) rats were double-housed under standard laboratory conditions and kept under a 12:12-hour light-dark schedule (lights on at 6:00 AM). Rats were weighed and dosed orally with a single administration of either vehicle control (0.5% methyl cellulose) or PF-05221304 ranging from 0.03 to 300 mg/kg. One hour after the dose, rats were dosed by intraperitoneal injection with [^{14}C] acetate (0.1 μCi/g body weight). One hour after the [^{14}C] acetate dose, rats were killed by CO_2 asphyxiation. Blood was collected via cardiac puncture. Livers were collected into preweighed Pyrex (Corning) tubes containing 2.5 mol/L NaOH. The procedure for extracting lipid and evaluating DNL synthesis was derived from a previously published method.[8] DNL for each sample was determined

by measuring ^{14}C incorporation into lipids, reported as disintegrations per minute/100 mg of tissue.

Effects of PF-05221304 on Inhibition of De Novo Lipogenesis in Western Diet–Fed Rats

Male Sprague-Dawley (~200 g) rats were double-housed under standard laboratory conditions and kept under a 12:12-hour reverse light-dark schedule (lights off at 8:00 AM). Rats were randomized into chow or Western diet (Research Diets; D12079B, New Brunswick, NJ) groups and given a 10-day lead-in period on diet before starting the study. Starting on day 1 of the study, rats were dosed orally with either vehicle control (0.25% MC) or PF-05221304 at 1, 3, or 10 mg/kg for 28 days. Rats were weighed twice weekly throughout the study. Seven days before the end of study, rats were dosed orally (20 mL/kg,) with 99% D_2O to achieve an approximately 5% D_2O body water enrichment. In addition, drinking water and dosing solutions then were enriched with 5% D_2O.

Rats were euthanized by CO_2 asphyxiation for tissue collection. Blood was collected via cardiac puncture. Livers were rapidly removed and freeze-clamped. Frozen livers were pulverized on a N_2 cooled aluminum block. Powdered liver was homogenized using lysing tubes containing homogenization buffer (10 mmol/L TRIS, pH 7.4, 0.9% NaCl, and 0.2% Triton X-100; Sigma Aldrich, St. Louis, MO), and immediately analyzed on a Siemens (Munich, Germany) Chemistry XPT clinical analyzer.

DNL was quantified by measuring the deuterium enrichment of body water and the incorporation of deuterium into palmitate in plasma. The fractional contribution of DNL to palmitate was calculated using established formulae.[35]

Body water deuterium enrichment was measured from plasma samples and quantified by Metabolic Solutions, Inc (Nashua, NH). Deuterium incorporation into plasma palmitate was measured using gas chromatography–MS methodology. Plasma lipids were extracted by the method of Bligh and Dyer,[36] followed by transesterification to fatty acid methyl esters with boron trifluoride/methanol, using the method of Morrison and Smith.[37] Fatty acid methyl esters were analyzed by gas chromatography–MS.

Acute Poloxomer 407 Challenge to Assess VLDL-TG Secretion

To determine the effects that ACC inhibition has on VLDL-TG secretion, jugular vein–cannulated male Sprague–Dawley rats (Envigo, Indianapolis. IN) were placed on either a chow (5053; Lab Diet, St. Louis, MO) or Western diet (12079bi; Research Diets) for 14 days before being administered vehicle (0.5% Methylcellulose in Deionized water) or PF-05221304 at 10 mg/kg for 7 days twice daily. On day 7 of dosing, animals were fasted for 3.5 hours before the final administration of compound. At time 0, 30 minutes after compound administration, animals were baseline bled before being administered an intravenous dose of Poloxomer (Sigma Aldrich) 407 (7% [v/v], 5 mL/kg). Blood was drawn via lateral tail vein at 30 minutes, 60 minutes, and 90 minutes after Poloxomer 407 administration and placed in an EDTA-coated tube for plasma analysis on a clinical analyzer.

Effect of PF-05221304 on Th17 Effector Cell Proliferation/Differentiation in Naïve Human T-Cells (CD4+ CD45RA+) Under Th17 Polarizing Conditions

Cryopreserved naïve human T cells isolated from cord blood (CD4+ CD45RA+) were thawed and washed according to the vendor's recommendations. MACS (Miltenyi Biotec, Bergisch Gladbach, Germany) T-cell activation beads against CD3, CD2, and CD28 then were added to the cells in a 1:1 bead:cell ratio. Cells were diluted in Lonza (Basel, Switzerland) X-VIVO 20 media and plated in 96-well, round-bottom plates (50,000 cells/well) and a cytokine cocktail (20 ng/mL IL1β, 30 ng/mL IL6, 30 ng/mL IL23, 5 ng/mL TGFβ1, 1 μg/mL anti–interferon-γ, and 2.5 μg/mL anti-IL4) was added to each well. PF-05221304 was dissolved in DMSO, serially diluted, and added to the cells. At 72 hours, a portion of the wells were harvested and lysed for gene expression. Human TaqMan (Applied Biosystems, Foster City, CA) probes against *FoxP3*, *IL17A*, and RAR-related orphan receptor C gene all were assessed using *Actb* as a housekeeping gene on quantitative polymerase chain reaction. Cells on other plates were allowed to continue differentiating with a change in media/cytokines/PF-05221304 on the third day and the fifth day. One plate did not receive a change in media on day 3. Media from this plate was assayed for secreted IL17 on day 5. On the morning of the sixth day, cells were washed and stimulated with a leukocyte activation cocktail with GolgiPlug (BD Biosciences, Woburn, MA) for 5 hours. After stimulation, cells were fixed, lysed and permeabilized, and stained with anti-human CD4 and IL17A–fluorescein isothiocyanate. Permeabilization/fixation and cytokine staining protocols were adopted from Miltenyi Biotec. All scatter plots were obtained on a MACSquant VYB flow cytometer and analyzed using MACSquantify software. By using a parallel 96-well plate, on day 6, 0.2 μCi of ^{14}C-acetate was added to the cells and incubated for 1 hour. Upon termination of the experiment, cells were lysed and cell lysates were transferred to glass scintillation vials. The samples then were hydrolyzed and lipids were isolated by organic extraction. Radioactivity was determined using standard scintillation techniques.

Effects of Chronic Oral Administration of PF-05221304 on the Development of Hepatic Inflammation in DEN-Treated Rats

Male Sprague–Dawley rats (~200 g) were pair-housed under standard laboratory conditions and kept on a 12:12-hour reverse light-dark schedule (lights off at 8:00 AM). Rats were randomized into saline (control) or DEN treatment groups and vehicle or PF-05221304. Starting on day 1 of the study, rats were administered DEN once weekly by intraperitoneal injection (50 mg/kg) to induce hepatic inflammation and were dosed orally with either vehicle control (0.25% methyl cellulose) or 10 mg/kg PF-05221304 (once a day) for 13 weeks. Rats administered saline once weekly by intraperitoneal injection and vehicle once daily by oral gavage for 13 weeks were used as a control. Rats were weighed twice weekly throughout the study and dosing volumes were adjusted accordingly. On the last day of the study, 1 week

after the last DEN injection, blood was collected via lateral tail vein. After blood collection, rats were euthanized by CO_2 asphyxiation. Plasma samples were analyzed on a Siemens Chemistry XPT clinical analyzer.

Livers were rapidly removed, weighed, and the left lateral lobe was excised and approximately 3-mm sections were placed into 10% neutral buffered formalin and processed to paraffin blocks using standard tissue processing protocols for histology. The remainder of the liver was freeze-clamped. Frozen livers then were rapidly pulverized on a liquid N_2 cooled aluminum block. Pulverized liver was homogenized and hepatic TG concentration was determined as described earlier. Formalin-fixed, paraffin-embedded liver sections were used for αSMA and CD3 IHC. Five-micron sections were cut using a rotary microtome and mounted on glass slides. Slides then were deparaffinized and rehydrated. Antigen retrieval was performed using a pH 6 solution of citric acid (Biogenex, Freemont, CA) for αSMA and Rodent Decloaker Solution (Biocare Medical, Concord, CA) for CD3 and loaded into the Biocare Medical Decloaking Chamber NxGENTM. Immunohistochemistry staining was completed on the Biocare Medical IntelliPATH automated IHC instrument using the following protocol: endogenous peroxidase was blocked by incubating with a 3% solution of hydrogen peroxide for 10 minutes, and nonspecific binding sites were blocked by applying Rodent Block R (Biocare Medical) for 20 (αSMA) or 30 (CD3) minutes. Anti-αSMA (clone 1A4, 71 μg/mL; Dako, Carpinteria, CA) at a dilution of 1:100, 0.71 μg/mL and anti-CD3 (clone SP7; Thermo Fisher Scientific, Waltham MA) at a dilution of 1:250, were incubated for 60 minutes at room temperature and detected by applying a mouse on rat for 30 minutes (αSMA) or rabbit anti-rodent for 20 minutes (CD3) HRP Polymer (Biocare Medical), followed by visualization with the 3,3′-diaminobenzidine (DAB) (Dako) for 5 minutes. Slides then were removed from the IntelliPATH and counterstained with Mayer's hematoxylin (Dako) and mounted with a permanent mounting medium. For each assay, a subset of duplicate liver slides were run as negative controls. These slides were incubated with a mouse IgG2a isotype control, run at a dilution of 1:250, 1.0 μg/mL (clone C1.18.4, 250 μg/mL; BD Biosciences, San Jose CA) for αSMA or a rabbit IgG isotype control run at a dilution of 1:1000, 5.0 μg/mL (polyclonal, 5 mg/mL; Vector Labs, Burlingame, CA) for CD3 for 60 minutes at room temperature.

Images of the αSMA and CD3 IHC slides were captured using the Aperio AT2 scanner (Leica Biosystems, Buffalo Grove, IL) at 20× magnification and images were saved in .svs format and stored in the Aperio eslide Manager image database (Leica Biosystems). Quantification of αSMA and CD3 IHC area percentage (DAB-positive area/total tissue region of interest × 100) was performed using the Definiens Tissue Studio Image Analysis Software (Carlsbad, CA). A threshold for αSMA and CD3 IHC DAB-positive area was applied to the liver tissue identified (region of interest) and measurements (DAB-positive area and total liver area [region of interest]) were exported to Microsoft Excel (Microsoft Corporation, Redmond, WA) for IHC area percentage calculation.

Effect of PF-05221304 on Hepatic Stellate Cell Activation

The effect of PF-05221304 to inhibit activation of hepatic stellate cells to a fibrogenic myofibroblast was assessed by measuring the effect of the compound on the production of αSMA and collagen from primary hepatic stellate cells stimulated with TGFβ1 to drive fibrogenesis. Briefly, human hepatic stellate cells (cat 5300; Sciencell Research Laboratories, Carlsbad, CA) were treated with 1 ng/mL TGFβ1 (cat 240B; R&D Systems, Minneapolis, MN) in the presence of varying concentrations of PF-05221304 or vehicle. Ascorbic acid was added at 100 μmol/L to the cell culture media to enhance the collagen production. Hepatic stellate cells unstimulated with TGFβ1 were used as a control. After a 72-hour incubation, the wells were methanol fixed, blocked, and incubated with anti-αSMA (clone 1A4; Sigma Aldrich) and anti-Col1A1 (cat C2456; Sigma), followed by matching secondary antibodies and Hoechst (Invitrogen, Carlsbad, CA) to produce an immunofluorescence signal. The cells were imaged on an Opera Phenix High Content Imaging platform (PerkinElmer). Images were analyzed with custom scripts in Columbus (PerkinElmer) for αSMA and collagen fluorescence intensity and nuclear counts. Effects on TGFβ1-stimulated proliferation was assessed by comparing the nuclear cell density of compound-treated cells to TGFβ1-stimulated vehicle-treated cells and the unstimulated control cells.

Effect of PF-05221304 on De Novo Lipogenesis in Human Stellate Cells

The effect of PF-05221304 on DNL in primary human stellate cells was assessed by measuring the incorporation of ^{14}C-acetate in newly formed lipid. After a 1-hour incubation of plated confluent human stellate cells (cat. 5300; Sciencell Research Laboratories) with varying concentrations of PF-05221304 or vehicle, ^{14}C-acetate (cat. ARC0158B; American Radiolabeled Chemicals, St. Louis, MO) was added and incubated for an additional 2 hours. The cells were washed with phosphate-buffered saline and hydrolyzed/saponified by heating with sodium hydroxide at 60°C. Ethanol and petroleum ether were added, centrifuged, and the organic phase was discarded. Fatty acids were extracted with petroleum ether after the addition of hydrochloric acid. The organic phase was dried under nitrogen gas and radiolabeled fatty acids were assayed using standard scintillation techniques.

Effects of PF-05221304 on Progression of Hepatic Inflammation and Fibrosis in Choline-Deficient and High-Fat Diet–Fed Rats

The effects of chronic oral administration of PF-05221304 on the progression of hepatic inflammation and fibrosis were evaluated in CDAHFD-fed rats. Briefly, male Wistar Han rats (~200 g) were double-housed under standard laboratory conditions and kept under a 12:12-hour reverse light-dark schedule (lights off at 8:00 AM). Rats were randomized into chow or CDAHFD groups at arrival

and were given a 6-week lead-in period on the respective diet before starting the study. Before starting the study, baseline blood collection and shear wave elastography (SWE) readings were conducted to randomize rats into treatment groups. SWE was performed using an Aixplorer Ultimate system (SuperSonic Imagine, Aix-en-Provence, France) with a 6- to 20-MHz linear array (SuperLinear SLH20-6; SuperSonic Imagine, Aix-en-Provence, France) transducer. All animals were fasted for approximately 4 to 6 hours to minimize interference of gut contents and gut movement during image acquisition. Starting on day 1 of the study, rats were dosed orally with either vehicle control (0.5% MC, twice daily) or PF-05221304 at 5 mg/kg (twice daily) for 6 weeks. Rats were weighed twice weekly throughout the study. An interim bleed and SWE was conducted at week 3 of treatment. A final SWE reading was performed during the last week of the study. Plasma samples were analyzed on a Siemens Chemistry XPT clinical analyzer. Frozen livers were pulverized on a N_2 cooled aluminum block.

On the last day of the study, blood was collected via tail vein and rats were euthanized by CO_2 asphyxiation for tissue collection. Plasma samples were analyzed on a Siemens Chemistry XPT clinical analyzer. Plasma monocyte chemoattractant protein 1 levels were analyzed using a Meso Scale Discovery biomarker assay.

Livers were rapidly removed and the right lateral, medial, and left lateral lobes of the liver were excised and approximately 3-mm sections were placed in 10% neutral buffered formalin and processed to paraffin blocks using standard tissue processing protocols for histology. Formalin-fixed paraffin-embedded liver sections were used for αSMA IHC and PSR histochemical staining. Five-micron (αSMA) and 7-μm (PSR) sections were cut using a rotary microtome and mounted on glass slides. For αSMA IHC, slides were placed on the Bond RX Fully Automated Research Stainer (Leica Biosystems) where they were automatically deparaffinized and rehydrated. Epitope retrieval was completed on all of the slides using the Leica ER1 (H1), pH 6, citrate solution for 20 minutes, then the slides were stained using a Leica Bond Polymer Refine DAB Detection Kit (DS9800). αSMA staining was completed using the following protocol: refine the hydrogen peroxide/endogenous peroxidase block for 10 minutes and blocking of nonspecific binding sites by Serum-Free Protein Block (Agilent, Santa Clara CA) for 10 minutes. Primary antibody incubation of anti-αSMA (clone 1A4, 20 mg/mL; R&D Systems) at 1:500 (0.04 ug/mL) for 15 room temperature, followed by polyclonal rabbit anti–Alexa Fluor 488 (1 mg/mL; Life Technologies, Carlsbad, CA) incubation for 10 minutes at 1:500 (2 ug/mL), Refine Polymer Detection for 8 minutes, Mixed Refine DAB for 5 minutes, and Leica Refine Hematoxylin counterstain for 5 minutes. Slides then were removed from the Leica Bond RX, dehydrated through graded alcohols to xylene, and coverslipped with permanent mounting media. For each αSMA assay, a subset of duplicate liver slides was run as negative controls. These slides were stained following the same protocol as described earlier, but incubated with mouse IgG2a–Alexa Fluor–conjugated isotype control (50 mg/mL; R&D Systems) run at a dilution of 1:1250 (0.04 μg/mL) for 15 minutes at room temperature. For PSR (cat. F-357-2; Rowley Biochemical, Inc, Danvers, MA), slides were stained by semiautomation using Tissue-Tek Prisma Plus (Sakura Finetek USA, Inc, Torrance, CA). Slides were deparaffinized and placed overnight in Bouin fluid before returning to the stainer and stained as per the manufacturer's protocol with some optimized steps (1% phosphomolybdic acid for 5 minutes; 0.1% Sirius Red in saturated Picrid acid for 90 minutes; 2 × 30-second wash in 0.5% acetic acid). Slides were automatically dehydrated and then mounted with a permanent mounting medium.

Images of the αSMA IHC and PSR-stained slides were captured using the Aperio AT2 scanner (Leica Biosystems) at 20× magnification and were saved in .svs format and stored in Aperio eslide Manager image database (Leica Biosystems). Images were analyzed using custom algorithms created in VISIOPHARM software (Visiopharm, Hoersholm, Denmark). VISIOPHARM applications with threshold parameters were applied uniformly to identify and quantify the liver sections area, αSMA IHC (DAB-positive area), and PSR stain area. Measurements were exported to Microsoft Excel (Microsoft Corporation) for area percentage calculations. A portion of the liver also was freeze-clamped and pulverized on a N_2 cooled aluminum block. An aliquot of the pulverized liver was homogenized using lysing tubes containing homogenization buffer (10 mmol/L TRIS, pH 7.4, 0.9% NaCl, and 0.2% Triton X-100), and immediately analyzed on a Siemens Chemistry XPT clinical analyzer to quantify hepatic TG levels. An additional aliquot of the pulverized liver was processed and analyzed for inflammatory and fibrotic gene expression. Rat TaqMan probes against α-SMA, Col1a1, CCL2, and Col3a1 all were assessed using Actb as the housekeeping gene on quantitative polymerase chain reaction.

Statistical Analysis

All data are reported as the means ± SEM. Intergroup treatment effects in the Western diet rat study were assessed using 1-way analysis of variance with the post hoc Dunnett test for multiple comparisons as appropriate for normally distributed data sets. Statistical significance was set at 0.05. For all additional studies, which used a single dose level of PF-05221304, the treatment effect of PF-05221304, relative to vehicle-administered animals, was analyzed using an exact Mann–Whitney rank-sum nonparametric test. Statistical significance was set at 0.05. SWE data were analyzed using a mixed-effect model repeat measurement with regimen, week, and regimen * week interaction as fixed factors, and animal as a random factor. Least-squares means estimates, least-squares means differences between regimens at each time point, along with their respective 95% CI and *P* values were calculated. Statistical significance was set at 0.05.

References

1. Sanyal AJ, Friedman SL, McCullough AJ, Dimick-Santos L, American Association for the Study of Liver D, United States F, Drug A. Challenges and opportunities in drug and biomarker development for nonalcoholic steatohepatitis: findings and recommendations from an American Association for the Study of Liver Diseases–U. S. Food and Drug Administration Joint Workshop. Hepatology 2015;61:1392–1405.
2. Fiorucci S, Biagioli M, Distrutti E. Future trends in the treatment of non-alcoholic steatohepatitis. Pharmacol Res 2018;134:289–298.
3. Cohen JC, Horton JD, Hobbs HH. Human fatty liver disease: old questions and new insights. Science 2011; 332:1519–1523.
4. Lambert JE, Ramos-Roman MA, Browning JD, Parks EJ. Increased de novo lipogenesis is a distinct characteristic of individuals with nonalcoholic fatty liver disease. Gastroenterology 2014;146:726–735.
5. Saggerson D. Malonyl-CoA, a key signaling molecule in mammalian cells. Annu Rev Nutr 2008;28:253–272.
6. Waite M, Wakil SJ. Studies on the mechanism of fatty acid synthesis. XII. Acetyl coenzyme A carboxylase. J Biol Chem 1962;237:2750–2757.
7. McGarry JD, Mannaerts GP, Foster DW. A possible role for malonyl-CoA in the regulation of hepatic fatty acid oxidation and ketogenesis. J Clin Invest 1977; 60:265–270.
8. Harwood HJ Jr, Petras SF, Shelly LD, Zaccaro LM, Perry DA, Makowski MR, Hargrove DM, Martin KA, Tracey WR, Chapman JG, Magee WP, Dalvie DK, Soliman VF, Martin WH, Mularski CJ, Eisenbeis SA. Isozyme-nonselective N-substituted bipiperidylcarboxamide acetyl-CoA carboxylase inhibitors reduce tissue malonyl-CoA concentrations, inhibit fatty acid synthesis, and increase fatty acid oxidation in cultured cells and in experimental animals. J Biol Chem 2003; 278:37099–37111.
9. Savage DB, Choi CS, Samuel VT, Liu ZX, Zhang D, Wang A, Zhang XM, Cline GW, Yu XX, Geisler JG, Bhanot S, Monia BP, Shulman GI. Reversal of diet-induced hepatic steatosis and hepatic insulin resistance by antisense oligonucleotide inhibitors of acetyl-CoA carboxylases 1 and 2. J Clin Invest 2006; 116:817–824.
10. Berod L, Friedrich C, Nandan A, Freitag J, Hagemann S, Harmrolfs K, Sandouk A, Hesse C, Castro CN, Bahre H, Tschirner SK, Gorinski N, Gohmert M, Mayer CT, Huehn J, Ponimaskin E, Abraham WR, Muller R, Lochner M, Sparwasser T. De novo fatty acid synthesis controls the fate between regulatory T and T helper 17 cells. Nat Med 2014;20:1327–1333.
11. Rau M, Schilling AK, Meertens J, Hering I, Weiss J, Jurowich C, Kudlich T, Hermanns HM, Bantel H, Beyersdorf N, Geier A. Progression from nonalcoholic fatty liver to nonalcoholic steatohepatitis is marked by a higher frequency of Th17 cells in the liver and an increased Th17/resting regulatory T cell ratio in peripheral blood and in the liver. J Immunol 2016; 196:97–105.
12. Bergman A, Carvajal-Gonzalez S, Tarabar S, Saxena AR, Esler WP, Amin NB. Safety, Tolerability, Pharmacokinetics, and pharmacodynamics of a liver-targeting acetyl-CoA carboxylase inhibitor (PF-05221304): a three-part randomized phase 1 study. Clin Pharmacol Drug Dev 2020;9:514–526.
13. Goedeke L, Bates J, Vatner DF, Perry RJ, Wang T, Ramirez R, Li L, Ellis MW, Zhang D, Wong KE, Beysen C, Cline GW, Ray AS, Shulman GI. Acetyl-CoA carboxylase inhibition reverses NAFLD and hepatic insulin resistance but promotes hypertriglyceridemia in rodents. Hepatology 2018;68:2197–2211.
14. Giannini EG, Testa R, Savarino V. Liver enzyme alteration: a guide for clinicians. CMAJ 2005;172:367–379.
15. Kim CW, Addy C, Kusunoki J, Anderson NN, Deja S, Fu X, Burgess SC, Li C, Ruddy M, Chakravarthy M, Previs S, Milstein S, Fitzgerald K, Kelley DE, Horton JD. Acetyl CoA carboxylase inhibition reduces hepatic steatosis but elevates plasma triglycerides in mice and humans: a bedside to bench investigation. Cell Metab 2017;26:576.
16. Lawitz EJ, Coste A, Poordad F, Alkhouri N, Loo N, McColgan BJ, Tarrant JM, Nguyen T, Han L, Chung C, Ray AS, McHutchison JG, Subramanian GM, Myers RP, Middleton MS, Sirlin C, Loomba R, Nyangau E, Fitch M, Li K, Hellerstein M. Acetyl-CoA carboxylase inhibitor GS-0976 for 12 weeks reduces hepatic de novo lipogenesis and steatosis in patients with nonalcoholic steatohepatitis. Clin Gastroenterol Hepatol 2018;16:1983–1991.
17. Amin N, Carvajal Gonzalez S, Aggarwal N, Tuthill T, Inglot M, Bergman A, Esler WP. PF-05221304 (PF'1304), a liver-targeted acetyl-coa carboxylase inhibitor (ACCi), in adults with nonalcoholic fatty liver disease (NAFLD) demonstrates robust reductions in liver fat and ALT – phase 2a, dose-ranging study. Hepatology 2019; 70(Suppl):21A.
18. Hoehn KL, Turner N, Swarbrick MM, Wilks D, Preston E, Phua Y, Joshi H, Furler SM, Larance M, Hegarty BD, Leslie SJ, Pickford R, Hoy AJ, Kraegen EW, James DE, Cooney GJ. Acute or chronic upregulation of mitochondrial fatty acid oxidation has no net effect on whole-body energy expenditure or adiposity. Cell Metab 2010; 11:70–76.
19. Griffith DA, Kung DW, Esler WP, Amor PA, Bagley SW, Beysen C, Carvajal-Gonzalez S, Doran SD, Limberakis C, Mathiowetz AM, McPherson K, Price DA, Ravussin E, Sonnenberg GE, Southers JA, Sweet LJ, Turner SM, Vajdos FF. Decreasing the rate of metabolic ketone reduction in the discovery of a clinical acetyl-CoA carboxylase inhibitor for the treatment of diabetes. J Med Chem 2014;57:10512–10526.
20. Harriman G, Greenwood J, Bhat S, Huang X, Wang R, Paul D, Tong L, Saha AK, Westlin WF, Kapeller R, Harwood HJ Jr. Acetyl-CoA carboxylase inhibition by ND-630 reduces hepatic steatosis, improves insulin sensitivity, and modulates dyslipidemia in rats. Proc Natl Acad Sci U S A 2016;113:E1796–E1805.
21. Takagi H, Tanimoto K, Shimazaki A, Tonomura Y, Momosaki S, Sakamoto S, Abe K, Notoya M, Yukioka H.

A novel acetyl-CoA carboxylase 2 selective inhibitor improves whole-body insulin resistance and hyperglycemia in diabetic mice through target-dependent pathways. J Pharmacol Exp Ther 2020;372:256–263.

22. Loomba R, Kayali Z, Noureddin M, Ruane P, Lawitz EJ, Bennett M, Wang L, Harting E, Tarrant JM, McColgan BJ, Chung C, Ray AS, Subramanian GM, Myers RP, Middleton MS, Lai M, Charlton M, Harrison SA. GS-0976 reduces hepatic steatosis and fibrosis markers in patients with nonalcoholic fatty liver disease. Gastroenterology 2018;155:1463–1473 e6.
23. Nati M, Haddad D, Birkenfeld AL, Koch CA, Chavakis T, Chatzigeorgiou A. The role of immune cells in metabolism-related liver inflammation and development of non-alcoholic steatohepatitis (NASH). Rev Endocr Metab Disord 2016;17:29–39.
24. Chackelevicius CM, Gambaro SE, Tiribelli C, Rosso N. Th17 involvement in nonalcoholic fatty liver disease progression to non-alcoholic steatohepatitis. World J Gastroenterol 2016;22:9096–9103.
25. Swiderska M, Jaroszewicz J, Stawicka A, Parfieniuk-Kowerda A, Chabowski A, Flisiak R. The interplay between Th17 and T-regulatory responses as well as adipokines in the progression of non-alcoholic fatty liver disease. Clin Exp Hepatol 2017;3:127–134.
26. Pearce EL, Poffenberger MC, Chang CH, Jones RG. Fueling immunity: insights into metabolism and lymphocyte function. Science 2013;342:1242454.
27. Shi LZ, Wang R, Huang G, Vogel P, Neale G, Green DR, Chi H. HIF1alpha-dependent glycolytic pathway orchestrates a metabolic checkpoint for the differentiation of TH17 and Treg cells. J Exp Med 2011;208:1367–1376.
28. Michalek RD, Gerriets VA, Jacobs SR, Macintyre AN, MacIver NJ, Mason EF, Sullivan SA, Nichols AG, Rathmell JC. Cutting edge: distinct glycolytic and lipid oxidative metabolic programs are essential for effector and regulatory CD4+ T cell subsets. J Immunol 2011;186:3299–3303.
29. Tsuchida T, Friedman SL. Mechanisms of hepatic stellate cell activation. Nat Rev Gastroenterol Hepatol 2017;14:397–411.
30. Beckers A, Organe S, Timmermans L, Scheys K, Peeters A, Brusselmans K, Verhoeven G, Swinnen JV. Chemical inhibition of acetyl-CoA carboxylase induces growth arrest and cytotoxicity selectively in cancer cells. Cancer Res 2007;67:8180–8187.
31. Jones JE, Esler WP, Patel R, Lanba A, Vera NB, Pfefferkorn JA, Vernochet C. Inhibition of acetyl-CoA carboxylase 1 (ACC1) and 2 (ACC2) reduces proliferation and de novo lipogenesis of EGFRvIII human glioblastoma cells. PLoS One 2017;12:e0169566.
32. Li S, Qiu L, Wu B, Shen H, Zhu J, Zhou L, Gu L, Di W. TOFA suppresses ovarian cancer cell growth in vitro and in vivo. Mol Med Rep 2013;8:373–378.
33. Svensson RU, Parker SJ, Eichner LJ, Kolar MJ, Wallace M, Brun SN, Lombardo PS, Van Nostrand JL, Hutchins A, Vera L, Gerken L, Greenwood J, Bhat S, Harriman G, Westlin WF, Harwood HJ Jr, Saghatelian A, Kapeller R, Metallo CM, Shaw RJ. Inhibition of acetyl-CoA carboxylase suppresses fatty acid synthesis and tumor growth of non-small-cell lung cancer in preclinical models. Nat Med 2016;22:1108–1119.
34. Petrova E, Scholz A, Paul J, Sturz A, Haike K, Siegel F, Mumberg D, Liu N. Acetyl-CoA carboxylase inhibitors attenuate WNT and Hedgehog signaling and suppress pancreatic tumor growth. Oncotarget 2017;8:48660–48670.
35. Guo ZK, Cella LK, Baum C, Ravussin E, Schoeller DA. De novo lipogenesis in adipose tissue of lean and obese women: application of deuterated water and isotope ratio mass spectrometry. Int J Obes Relat Metab Disord 2000;24:932–937.
36. Bligh EG, Dyer WJ. A rapid method of total lipid extraction and purification. Can J Biochem Physiol 1959;37:911–917.
37. Morrison WR, Smith LM. Preparation of fatty acid methyl esters and dimethylacetals from lipids with boron fluoride–methanol. J Lipid Res 1964;5:600–608.

Received November 14, 2019. Accepted June 2, 2020.

Correspondence
Address correspondence to: William P. Esler, PhD, Internal Medicine Research Unit, Pfizer, Inc, 1 Portland Street, Cambridge, Massachusetts 02139. e-mail: William.Esler@Pfizer.com.

Acknowledgments
The authors would like to thank Andrew Robertson, Lauren Martin, and Jennifer Ashley Travers for assistance with the histology slide preparation, and Gang Xing for measurement of malonyl-CoA levels. The authors also would like to thank Morrie Birnbaum for helpful discussions.

CRediT Authorship Contributions
William Paul Esler, PhD (Conceptualization: Equal; Funding acquisition: Equal; Investigation: Equal; Project administration: Lead; Supervision: Equal; Visualization: Equal; Writing – original draft: Lead; Writing – review & editing: Lead); Trenton T. Ross (Conceptualization: Equal; Data curation: Equal; Formal analysis: Equal; Funding acquisition: Equal; Investigation: Equal; Methodology: Equal; Supervision: Equal; Visualization: Equal; Writing – original draft: Supporting; Writing – review & editing: Lead) Collin Crowley (Data curation: Equal; Formal analysis: Equal; Investigation: Equal; Methodology: Equal; Validation: Equal; Writing – original draft: Supporting; Writing – review & editing: Equal) Kenneth L. Kelly (Conceptualization: Supporting; Data curation: Equal; Formal analysis: Equal; Methodology: Equal; Validation: Equal; Visualization: Equal; Writing – original draft: Supporting; Writing – review & editing: Equal) Anthony Rinaldi (Data curation: Equal; Formal analysis: Equal; Methodology: Equal; Validation: Equal; Writing – review & editing: Supporting) David A. Beebe (Conceptualization: Supporting; Formal analysis: Equal; Investigation: Equal; Methodology: Equal; Validation: Equal; Visualization: Equal; Writing – review & editing: Equal) Matthew P. Lech (Formal analysis: Equal; Investigation: Equal; Methodology: Equal; Validation: Equal; Visualization: Supporting; Writing – review & editing: Equal) Robert V. Martinez (Funding acquisition: Supporting; Investigation: Supporting; Methodology: Supporting; Resources: Supporting; Supervision: Supporting; Validation: Supporting; Writing – original draft: Supporting; Writing – review & editing: Equal) Santos Carvajal-Gonzalez (Conceptualization: Supporting; Data curation: Equal; Formal analysis: Lead; Methodology: Equal; Validation: Lead; Visualization: Equal; Writing – original draft: Supporting; Writing – review & editing: Equal) Magalie Boucher (Conceptualization: Supporting; Data curation: Supporting; Formal analysis: Equal; Investigation: Equal; Methodology: Equal; Supervision: Supporting; Validation: Equal; Visualization: Equal; Writing – original draft: Supporting; Writing – review & editing: Equal) Dinesh Hirenallur-Shanthappa (Data curation: Supporting; Formal analysis: Supporting; Investigation: Supporting; Methodology: Supporting; Validation: Equal; Visualization: Equal; Writing – review & editing: Equal) Jeffrey Morin (Data curation: Supporting; Formal analysis: Supporting; Methodology: Equal; Validation: Equal; Visualization: Equal; Writing – review & editing: Equal) Alan C. Opsahl (Data curation: Supporting; Formal analysis: Supporting; Methodology: Equal; Validation: Equal; Visualization: Equal; Writing – review & editing: Equal) Sarah R. Vargas (Data curation: Supporting; Formal analysis: Supporting; Methodology: Equal; Validation: Equal; Visualization: Equal; Writing – review & editing: Equal) Kendra K. Bence (Conceptualization: Supporting; Funding acquisition: Equal; Resources: Equal; Supervision: Equal; Writing – review & editing: Equal)

Jeffrey A. Pfefferkorn (Conceptualization: Supporting; Funding acquisition: Lead; Project administration: Supporting; Resources: Lead; Supervision: Equal; Writing – review & editing: Equal).

Conflicts of interest

The authors disclose the following: all authors are employees of Pfizer, Inc. The following authors are shareholders of Pfizer stock: Trenton T. Ross, David A. Beebe, Matthew P. Lech, Robert V. Martinez, Santos Carvajal-Gonzalez, Magalie Boucher, Dinesh Hirenallur-Shanthappa, Jeffrey Morin, Alan C. Opsahl, Sarah R. Vargas, Kendra K. Bence, Jeffrey A. Pfefferkorn, and William P. Esler.

Funding

This work was funded by Pfizer, Inc.